INFORMATION TO USERS

This manuscript has been reproduced from the microfilm master. UMI films the text directly from the original or copy submitted. Thus, some thesis and dissertation copies are in typewriter face, while others may be from any type of computer printer.

The quality of this reproduction is dependent upon the quality of the copy submitted. Broken or indistinct print, colored or poor quality illustrations and photographs, print bleedthrough, substandard margins, and improper alignment can adversely affect reproduction.

In the unlikely event that the author did not send UMI a complete manuscript and there are missing pages, these will be noted. Also, if unauthorized copyright material had to be removed, a note will indicate the deletion.

Oversize materials (e.g., maps, drawings, charts) are reproduced by sectioning the original, beginning at the upper left-hand corner and continuing from left to right in equal sections with small overlaps.

Photographs included in the original manuscript have been reproduced xerographically in this copy. Higher quality 6" x 9" black and white photographic prints are available for any photographs or illustrations appearing in this copy for an additional charge. Contact UMI directly to order.

Bell & Howell Information and Learning
300 North Zeeb Road, Ann Arbor, MI 48106-1346 USA
800-521-0600

Université d'Ottawa • University of Ottawa

PERMISSION DE REPRODUIRE ET DE DISTRIBUER LA THÈSE

PERMISSION TO REPRODUCE AND DISTRIBUTE THE THESIS

NOM DE L'AUTEUR / NAME OF AUTHOR:	DE ABREU, Robert
ADRESSE POSTALE / MAILING ADDRESS:	60 Fleury Chelsea, Québec J0X 1N0
GRADE / DEGREE:	**ANNÉE D'OBTENTION /YEAR GRANTED**
M.A.Sc.(Mechanical Engineering)	1999

TITRE DE LA THÈSE / TITLE OF THESIS:

Real-Time Damage Detection for Flexible Structures using Transient Vibrational Response

L'auteur permet, par la présente, la consultation et le prêt de cette thèse en conformité avec les règlements établis par le bibliothécaire en chef de l'Université d'Ottawa. L'auteur autorise aussi l'Université d'Ottawa, ses successeurs et cessionnaires, à reproduire cet exemplaire par photograhie ou photocopie pour fins de prêt ou de vente au prix coûtant aux bibliothèques ou aux chercheurs qui en feront la demande.

Les droits de publication par tout autre moyen et pour vente au public demeureront la propriété de l'auteur de la thèse sous réserve des règlements de l'Université d'Ottawa en matière de publication de thèses.

The author hereby permits the consultation and the lending of this thesis pursuant to the regulations established by the Chief Librarian of the University of Ottawa. The author also authorizes the University of Ottawa, its successors and assignees, to make reproductions of this copy by photographic means or by photocopying and to lend or sell such reproductions at cost to libraries and to scholars requesting them.

The right to publish the thesis by other means and to sell it to the public is reserved to the author, subject to the regulations of the University of Ottawa governing the publication of theses.

N.B. LE MASCULIN COMPREND ÉGALEMENT LE FÉMININ

March 26 '99
DATE

Robert DeAbreu
(AUTEUR) SIGNATURE (AUTHOR)

Université d'Ottawa · University of Ottawa

Université d'Ottawa · University of Ottawa

ÉCOLE DES ÉTUDES SUPÉRIEURES ET DE LA RECHERCHE

SCHOOL OF GRADUATE STUDIES AND RESEARCH

DE ABREU, Robert

AUTEUR DE LA THÈSE - AUTHOR OF THESIS

M.A.Sc.(Mechanical Engineering)

GRADE - DEGREE

Mechanical Engineering

FACULTÉ, ÉCOLE, DÉPARTEMENT - FACULTY, SCHOOL, DEPARTMENT

TITRE DE LA THÈSE - TITLE OF THE THESIS

Real-Time Damage Detection for Flexible Structures using Transient Vibrational Response

Dan Necsulescu

DIRECTEUR DE LA THÈSE - THESIS SUPERVISOR

EXAMINATEURS DE LA THÈSE - THESIS EXAMINERS

M. Liang

D. Gorman

J.Z. Sasiadek

J.-M. De Koninck, Ph.D.

LE DOYEN DE L'ÉCOLE DES ÉTUDES SUPÉRIEURES ET DE LA RECHERCHE

SIGNATURE

DEAN OF THE SCHOOL OF GRADUATE STUDIES AND RESEARCH

Real-Time Damage Detection for Flexible Structures Using Transient Vibrational Response

A thesis submitted to the
University of Ottawa
in partial fulfilment of the requirements
for the degree of

Master of Applied Science
in
Mechanical Engineering

By
©Robert De Abreu

Ottawa-Carleton Institute for Mechanical and Aerospace Engineering
University of Ottawa
Ottawa, Ontario, Canada, K1N 5N6

March 1999

National Library of Canada
Acquisitions and Bibliographic Services
395 Wellington Street
Ottawa ON K1A 0N4
Canada

Bibliothèque nationale du Canada
Acquisitions et services bibliographiques
395, rue Wellington
Ottawa ON K1A 0N4
Canada

Your file Votre référence

Our file Notre référence

The author has granted a non-exclusive licence allowing the National Library of Canada to reproduce, loan, distribute or sell copies of this thesis in microform, paper or electronic formats.

L'auteur a accordé une licence non exclusive permettant à la Bibliothèque nationale du Canada de reproduire, prêter, distribuer ou vendre des copies de cette thèse sous la forme de microfiche/film, de reproduction sur papier ou sur format électronique.

The author retains ownership of the copyright in this thesis. Neither the thesis nor substantial extracts from it may be printed or otherwise reproduced without the author's permission.

L'auteur conserve la propriété du droit d'auteur qui protège cette thèse. Ni la thèse ni des extraits substantiels de celle-ci ne doivent être imprimés ou autrement reproduits sans son autorisation.

0-612-45212-3

Canada

Dedicated to my Mother and Father,

Marian and Bernard De Abreu

Abstract

Flexible structures are often composed of a number of flexible parts connected together by rivets or bolts. Over time, the connections can become loose, creating a danger of structural integrity failure. During system operation, real-time monitoring to detect structural damage is required. In this thesis, a new non-destructive testing method to detect damage in structural connections using piezoelectric actuating/sensing devices is proposed. A thin beam with one end fixed and the other subjected to a variety of boundary conditions is used to investigate the feasibility of this method.

The method involves first flexurally exciting the beam and measuring its resulting transient vibrational response using piezoelectric devices, and then determining any change in its one variable boundary condition by comparing the measured response to that of a fixed-fixed (or secure) condition. The size of the difference in the responses indicates the extent of the boundary change. These differences are quantified by the use of damage indices. The proposed transient response approach uses information that cannot be obtained using current steady-state harmonic-based methods. Results of experiments and damage index analyses show that several of the differences in the transient responses of the beam are significantly and monotonically dependent on the level of damage of the connections.

Acknowledgements

I would like to express my gratitude to my supervisor, Dr. Dan S. Necsulescu, for his time, ideas, insight and guidance, which he supplied throughout the course of my thesis work. In addition, I thank him for sharing his wealth of career experience with me. His advice will certainly be useful as I start my career path.

I wish to express sincere thanks to my colleagues in the control lab, Bumsoo Kim and Rahim Jassemi, for their help, advice and encouragement.

I would like to acknowledge Sensor Technology of Collingwood, Ontario for supplying the piezo-ceramic sensors and actuators for the present research, and to thank Dr. Eswar Prasad and his employees for their time and for sharing their knowledge.

I would like to thank the members of my defence committee, Dr. D. Gorman, Dr. M. Liang and Dr. J. Sasiadek, for examining my thesis.

I would also like to thank Dr. Firooz Bakhtiari-Nejad, Friedhelm Altpeter, Jean DeCarufel, Mr. Byron Ostrom, Dr. Raj Singhal, and the academic members and staff of the Department of Mechanical Engineering, especially Dr. Michael Munro, Madan Makasari, Solange Lamontagne and Marie Rainville, for their help.

Lastly, I am very grateful to my parents for their sound advice, and continual support and encouragement.

Table of Contents

List of Figures

List of Tables

Nomenclature

a	coefficient
$a_n(s)$	n^{th} normal mode coefficient
$a(t)$	transverse acceleration of beam produced by the actuator at the actuator location
A	cross-sectional area
A_n	n^{th} mode shape constant
$b_n(s)$	n^{th} normal mode coefficient
B_n	n^{th} mode shape constant
C	capacitance
d	piezoelectric charge constant
d	matrix of piezoelectric charge constants
D	electric displacement
$\boldsymbol{D}$	electric displacement vector
E	elastic modulus
$\boldsymbol{E}$	electric field vector
$f(x,t)$	distributed force per unit length
F	force
F_c	normal force exerted by the clamp on the clamped end (variable boundary) of the beam
F_{secure}	normal force exerted by the clamp on the clamped end (variable boundary) of the beam in its secure state
g	piezoelectric voltage constant
G	shear modulus
I	moment of inertia of the cross-sectional area of the beam about its thickness axis
k	Timoshenko shear coefficient
K_L, K_t	constants relating voltage and deflection of a piezoelectric element
l	effective length of the beam in its secure (fixed-fixed) state
l_c	effective length of the beam in its disconnected (cantilever) state
l_a	distance along the length of the beam from the permanently fixed end to the centre point of the actuator
l_s	distance along the length of the beam from the permanently fixed end to the centre point of the sensor
L	length
ΔL	longitudinal elongation
N	number of samples
Q	electric charge
s	Laplace independent variable
s^E	compliance
$\boldsymbol{s}^E$	compliance matrix

S	strain matrix
t	thickness
t_b	thickness of the beam
t_{ex}	time at which the excitation of the beam is terminated
Δt	elongation in the thickness direction
$T_n(t)$	function
T	stress tensor
U	dummy variable
V	voltage
w	width of the beam
W	width
x	distance along the length of the beam from its permanently fixed end
$X_n(x)$	n^{th} flexural mode shape of the beam
$y(x,t)$	transverse (or flexural) displacement of the beam

Greek Symbols

α	amplitude of the sinusoidal flexural acceleration excitation to the beam
β_n	n^{th} wave number of the beam
δ	Dirac delta function
ϵ	dielectric permittivity constant
ϵ	dielectric permittivity constant matrix
ρ	density
σ	normal stress
Ω	excitation frequency in radians per second
ω	frequency in radians per second
ω_c	cutoff frequency in radians per second
ω_n	n^{th} natural frequency of the beam in radians per second

Chapter 1

Introduction

Aerospace structures are often composed of a large number of flexible parts or components which are connected together by fasteners such as rivets or bolts. These connections loosen over the operating life of the structures making real-time monitoring of their structural integrity a requirement for ensuring their safe operation. In addition to improving the reliability of these structures, another reason for developing a real-time approach is to minimize the time and cost involved in damage detection.

The field of real-time structural integrity monitoring is presently a very active area of research and is very applicable to the larger field of intelligent structures. Many approaches have been developed over the past number of years, each varying in the type of damage which they can detect, the speed at which they can detect the damage, and the type of dynamic-based information they use to detect the damage. Most of the research into real-time failure detection has employed piezoelectric actuators and sensors, mounted to the surface of the structure or embedded within the material of the structure, in order to generate mechanical waves and to measure the response without modifying

basic properties of the structures.

Many of the methods currently developed for monitoring the integrity of structures are based upon the steady-state vibrational response of the structure. So far, a small part of research has been devoted to using information contained in the transient response of the structure to mechanical excitations for the purpose of structural integrity monitoring. The primary objective of the research presented in this thesis was to develop a new real-time method for monitoring the structural integrity of flexible structures using transient vibrational response and piezoelectric devices. This new approach to damage detection uses information contained in the response of the structure that is not obtainable using the current steady-state harmonic response based approaches.

The thesis is organized as follows. An analytical model based on the Euler-Bernoulli theory is developed, in Chapter 3, for the transient flexural vibrational response of a flexible beam. In addition, simple analytical models for the piezoelectric elements, which are used to excite and measure mechanical vibrations in the beam, are developed. In Chapter 4, numerical simulations of the transient response of the beam, in both secure and disconnected states, to a finite number of sinusoidal flexural pulses are presented. In Chapter 5, the transient response of the beam to a similar excitation used in the simulations is investigated in experiment for the secure, disconnected and intermediate states of joint loosening in the beam. The differences observed in the responses of the various "damaged" states of the beam are quantified for real-time damage detection using a series of damage indices in Chapter 6. Conclusions and recommendations are given in Chapter 7.

Chapter 2

Literature Review

2.1 Intelligent Structures

Structural integrity monitoring is a very active research field in the domain of intelligent structures. Several overviews regarding intelligent structures have been published. In (Rogers 1990), an introduction to the area of intelligent structures is presented. Intelligent materials and sensors-actuators for intelligent structures is discussed in (Gandhi and Thomson 1992) but with little emphasis on algorithmic approaches. An extensive review of the technology of intelligent structures is given in (Crawley 1994).

Intelligent structures are the most advanced, but as yet unrealized, subset of much larger field of structures (Figure 2.1).

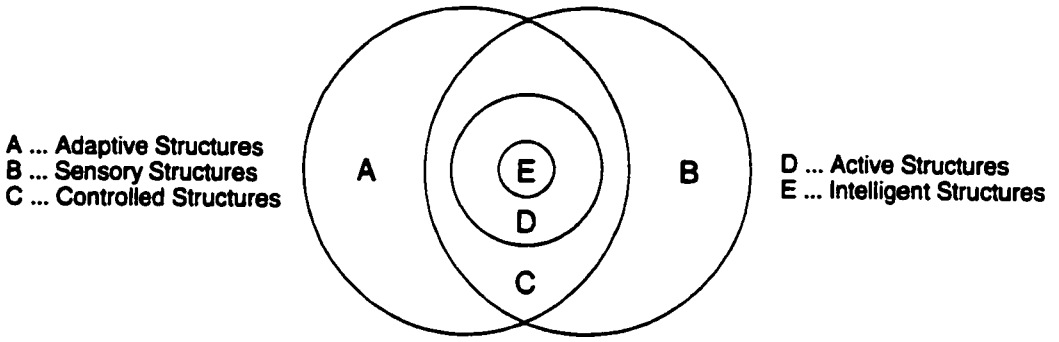

Figure 2.1: Classification of structures.

The various classes of structures, displayed in the above diagram, can be briefly explained as follows: adaptive structures have actuators distributed throughout; sensory structures have sensors distributed throughout; controlled structures contain actuators and sensors linked by closed loop control; and active structures are controlled structures which have highly distributed actuators which have structural functionality and participate in load-bearing (Crawley 1994).

An intelligent structure has the following characteristics: (1) it contains actuators and sensors that are highly integrated into the structure and modify, passively and actively, the dynamics of the structure; (2) it contains highly integrated controllers, signal conditioning and power amplification electronics; and (3) all of its actuating, sensing and signal processing elements serve the purpose of influencing the states or physical (e.g., mechanical, thermal, optical, chemical electrical or magnetic) characteristics of the structure (Crawley 1994).

Crawley identifies several component technologies which are critical to the evolution and application of intelligent structures. The following are discussed later in the context of structural integrity monitoring: actuators, sensors, and control methodologies and algorithms.

Some other applications resulting from the pursuit of an intelligent structure include shape control, robotic control, and vibration damping (Hagood and von Flotow 1991).

2.2 Structural Integrity Monitoring

In his 1990 overview of intelligent structures, Rogers presents the vision for the ideal health monitoring system for the aircraft of the future as one emulating the human nervous system. The propulsion, flight control avionics, and structural systems as well as subsystems of this "smart airplane" will all be monitored. Health monitoring of structural systems is the area addressed in this thesis. Several considerations influence the choice and effectiveness of a suitable structural health monitoring method (Housner et al. 1997).

The aim of monitoring the structural health (or integrity) of a system is to periodically detect, locate and quantify damage which may develop in the system over its operating life. Examples of possible damage include (not exclusively) cracks (Rizos et al. 1990), disconnections, delaminations (Islam and Craig 1994), voids (Cawley and Adams 1979), and loose connections (Lim et al. 1996; Pandey and Biswas 1994). In the proposed approach, damage is in the form of a loosening connection, although the use of the approach may be extended to other forms of damage.

Candidate structures for structural monitoring systems include civil structures (bridges, buildings, offshore platforms, dams, etc.), aerospace structures (aircraft, space vehicles and stations, etc.), and ground and sea vehicles (trains, ships, etc.). All these structures share common characteristics including complexity, high cost and large safety factors. Presently, the structures targeted in damage detection research have included simple structural components such as beams and plates, and simple structures such as trusses. The proposed approach is intended to be used on aerospace structures; the structure used for testing the approach is a thin beam.

One the earliest contributions to the field of structural integrity monitoring is (Adams et al. 1978). The authors identified the natural frequency of a structure as a useful parameter for damage detection since it varies with damage through changes in stiffness and damping, and it is independent of the point of excitation of the structure (except for vibration nodes). Using receptance analysis of the axial vibration on a rectangular bar, they were able to detect, locate and quantify analytically the damage in the bar. Damage was modelled as an ideal spring of varying stiffnesses. Experiments confirmed their findings. The analytical work was later extended using a finite element model (FEM) in order to realize detection of damage (in the form of a rectangular hole) in a thin plate (Cawley and Adams 1979).

Many characteristics of the vibrational response of the structure have been studied for use in damage detection. In (Pandey and Biswas 1994), natural frequencies were used to detect damage; however, damage was located and quantified through changes in flexibility rather than stiffness. Damage in a two section steel beam was realised in experiment by loosening the bolts of the

connection of the two sections of the beam. In (Pandey et al. 1991), changes in curvature mode shapes were used instead of natural frequencies for detecting and accurately locating cracks in a finite element model of a beam. The crack was modelled as a local reduction in the modulus of elasticity. Many researchers have used the eigenstructure (i.e., eigenvalues and eigenvectors) of the tested system to detect damage (Lim and Kashangaki 1994; Lim 1995; Kaouk and Zimmerman 1994).

All these approaches rely on the steady-state response of the structure. The transient response is used in the present approach since it contains additional information regarding the integrity of the structure.

Several general classes of methods have been researched over the past thirty years. These include model updating and system identification techniques, signature analysis and pattern recognition approaches, and neural network methods. Much of the published research in the past decade has been in the area of model updating.

Model Updating and System Identification

Model-based damage detection methods use a finite element model (FEM) of the system modal response coupled with experimental modal data to determine damage location and extent. In this approach, a refined FEM is first established for the original undamaged structure. Its analytical modal properties (i.e., natural frequencies, mode shapes) are in agreement with the corresponding

measured properties of the actual structure. Then, at predetermined intervals over the operating life of the structure, further measurements of the structural properties are taken. The new measurements are used to update the model so that the modal properties of the present state of the structure again correspond to those of the FEM, subject to various constraints (such as symmetry or sparsity preservation). Through updating the model, damage to the structure is located and quantified by determining changes to the stiffness and/or mass properties that would account for the observed differences in the measured modal properties.

Modelling errors, measurement noise and insensitivity of modal properties to local stiffness changes cause this to be an ill-conditioned, often non-unique, inverse problem (Housner et al. 1997). Even small modelling errors can result in the indication of "ghost damages" (Fritzen et al. 1997). In addition, the computation involved in these types of approaches is both intensive and expensive, and may make them unsuitable for real-time detection. Also, the effectiveness of these methods is limited when the damage is small (Cattarius and Inman 1997).

Research in this area can be separated into three separate classes of methods. In the first class, optimal matrix updating methods, a minimal modification is made to the original system model (i.e., matrices) so that the refined model can reproduce the measured modal data to some accuracy (Brock 1968; Kabe 1985; Doebling 1996). In the second class, sensitivity-based methods, the derivatives of the modal parameters (e.g., eigenvalues and/or eigenvectors) with respect to changes in physical design parameters are used as sensitivity coefficients. These coefficients are used for calculating the changes in the physical design parameters responsible for the discrepancy between the modal

parameters of the model and those which were measured for the actual system (Fritzen et al. 1997). In the third class, eigenstructure assignment methods, the eigenstructure of the system is used in locating and quantifying damage present in the structure (Lim and Kashangaki 1994; Lim 1995; Kaouk and Zimmerman 1994).

Neural Networks

Recently, damage detection approaches utilising neural networks have been receiving growing attention (Tsou and Herman Shen 1994; Islam and Craig 1994; Manning 1994). The process of damage identification is divided into two phases: (1) pattern generation and training, and (2) pattern recognition. Any of the types of the measured data discussed in this present section of the thesis can be used in the identification process. An advantage of approaches of this type is that no parametric model of the system is needed. However, extensive training of the neural network is required before reliable results can be obtained in damage detection.

Signature Analysis or Pattern Recognition

In this approach, changes in the "signature" (i.e., dynamic characteristics) of the structure are used to detect damage. The damage is then located by comparing the observed changes with a database of possible changes. A good example of this approach is presented in (Juneja et al. 1997). The authors used optimal excitations and frequency signatures, in combination, to locate and quantify the damage in a space truss, in simulation and experiment, by matching the excitations and

signatures to those present in a database of damage scenarios.

The proposed approach can be categorized in this class; however, since the damage is assumed to be located at the structural connection, a database is not employed. Some research in the literature was found to be representative. Rogers and collaborators developed an impedance-signature-based method (Liang et al. 1994a and 1994b; Sun et al. 1994) for use in damage detection. They later used the method to detect damage in a truss (Sun et al. 1995). Using several piezo-ceramic elements, each bonded to a truss node, the local mechanical impedance of the truss was measured indirectly through electric admittance. In a more recent paper (Giurgiutiu and Rogers 1997), the impedance-signature-based method was combined with wave propagation theory to detect damage. In (Jian et al. 1997), the authors used an impulse excitation and compared frequency signatures in detecting damage in a thin composite plate.

A desired quality of a structural integrity monitoring approach is real-time damage detection. The signature-based method presented in (Juneja et al. 1997) and the comprehensive model-updating approach presented in (Lim et al. 1996) represent two good examples of real-time detection. Two important factors in realizing real-time detection are the amounts of measurement and computation time required for the process.

All the papers mentioned so far in Section 2.2 use steady-state frequency-domain information, in terms of natural frequencies and/or mode shapes, for damage detection. Only a small amount of research has looked into exploiting the transient time-domain vibrational response of the

structure to identify damage. In a recently published paper (Cattarius and Inman 1997), the authors proposed a method which uses the transient response in the time domain and the phenomenon of beating in order to detect, analytically, damage in a beam. Experimental verification was carried out for a plate and a helicopter rotor blade. The tested structure was excited into vibration near one of its natural frequencies and then the excitation was removed and the free vibrational response of the beam was measured and subtracted from that of the undamaged signature response. If damage had occurred, a decrease in stiffness (or an increase in mass) was present which caused a decrease in the natural frequencies that was exaggerated in the difference of the two time responses by the presence of beats. The smaller the time interval between beats was, the greater was the damage. One drawback of this method is that it is time consuming, especially for small amounts of damage. A strength of a method of this type is, however, that no a priori knowledge of a model or development of a model is necessary.

The time domain approach proposed in this thesis is similar in some aspects to the research mentioned above in that the excitation is chosen to be near to a natural frequency of the structure and that no model is needed; however, instead of using beats, other characteristics (such as amplitude and decay duration of the response) are used as damage indicators. Use of these characteristics reduces the time involved in detection lending the approach to be perhaps more applicable to real-time monitoring. The model presented in Chapter 3 is used for simulation tests, but is not part of the real-time method tested in experiments. Preliminary results of the approach were published in (Necsulescu and DeAbreu 1998; Necsulescu et al. 1998).

2.3 Sensors and Actuators Used in Damage Detection

Several actuating technologies (e.g., piezoelectric, shape memory, magnetostrictive, electrostrictive and thermal materials, and electro-rheological fluids) and sensing technologies (e.g., strain gauges, fibre-optic sensors, and piezoelectric and shape memory materials) exist for intelligent structures (Gandhi and Thomson 1992); however, in the vast majority of damage detection research, piezoelectric materials, mounted to the tested structure, are employed to excite and sense mechanical vibrations.

Piezoelectric elements are able to transform mechanical energy into electrical energy and, conversely, electrical energy into mechanical energy, which makes them suitable as sensors and actuators, respectively, in the context of damage detection. In the former transformation, the direct piezoelectric effect, mechanical deformation (i.e., strain) applied to the element causes a proportional charge to be generated in the sensor material thus producing a definite voltage between the electrodes of the element. In the latter transformation, the converse piezoelectric effect, an applied electrical field induces strain in the element. (Doebelin 1990; Gandhi and Thomson 1992)

Linearized constitutive relations describing piezoelectric behaviour is published in (Standards Committee of the IEEE Ultrasonics, Ferroelectrics, and Frequency Control Society 1987). Using these relations, several researchers have developed models to account for the interaction present between piezo-elements and their host structures. In the previously mentioned (Sec. 2.2) research by Rogers and collaborators (Liang et al. 1994a and 1994b; Sun et al. 1994), a generic

electromechanical model which incorporated the mechanical impedance of the actuator and the structure (as a mass, spring and damper) was used to represent the dynamic interaction between the actuator and the structure. In (Hagood et al. 1990), the effects of dynamic coupling between a structure and an electrical network consisting of piezoelectric elements and passive electronics was modelled. In (de Benedetti and Barboni 1998), the constitutive relations were reduced to a system of two second order differential equations, which showed the coupling role of the electromechanical characteristics of piezoelectric elements. In Chapter 3 of this thesis, a simple model is developed to describe, in more detail, the operation of a piezoelectric element. However, for simulations, another form of this model was used, based on acceleration rather than force input.

Chapter 3

Analytical Model

3.1 Purpose

The motivation for developing an analytical model of a beam and performing numerical simulations of its response was to prove the concept of the proposed damage detection approach (i.e., that changes in the boundary conditions of a flexible structure can be detected by resulting differences in its transient vibrational responses).

3.2 Physical Model

The damage situations for the horizontal beam (fixed at both ends and equipped with a piezoceramic actuator and sensor) investigated in the development and testing of the proposed approach can be categorized into the following cases (Fig. 3.1):

I. Secure Beam - the beam has fixed connections at both ends

II. Disconnected Beam - the beam has developed a broken connection at one of its ends

III. Damaged Beam - the beam has developed a loose connection at one of its ends

The beam is made of aluminum and is of length l (in its secure state), width w and thickness t_b.

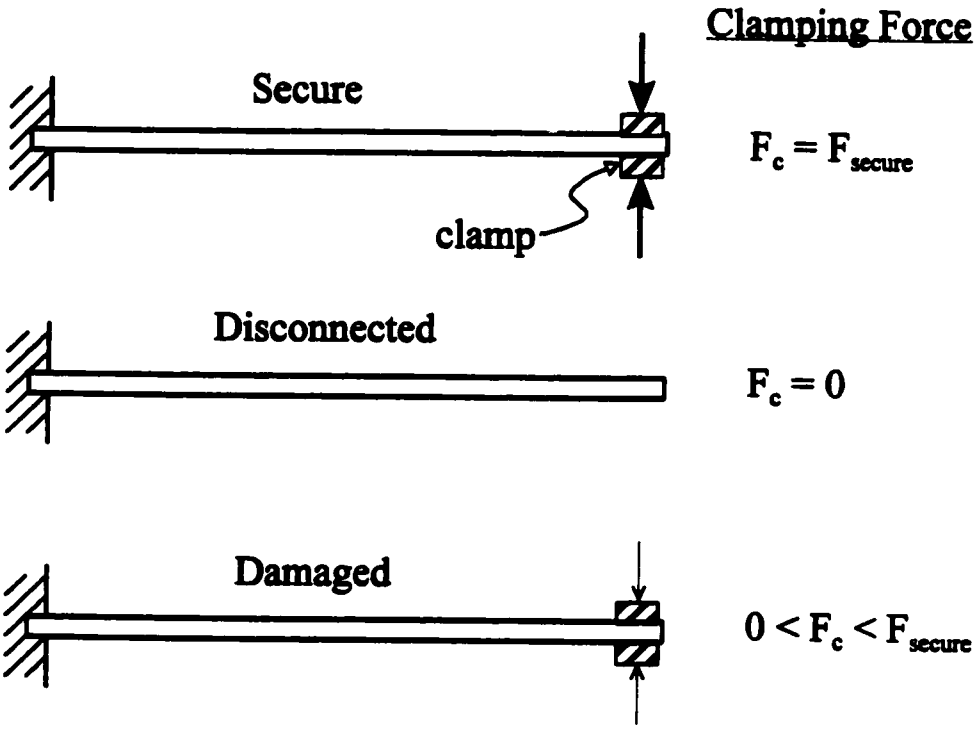

Figure 3.1: Limiting cases of joint loosening.

Given its purpose (Sec. 3.1), the analytical model should represent the two limiting cases of joint loosening: Cases I and II. The practical cases (i.e., damaged beam cases) where the joint has loosened but is not free, can be approximated by corresponding reductions in the clamping force F_c

at the loosened joint (Fig. 3.1). These more significant intermediate cases, along with the two extreme cases, were studied in experiment (Chapter 5).

3.3 Physical Description of the Beam

A thin aluminum beam equipped with an actuator and a sensor is shown in Figure 3.2.

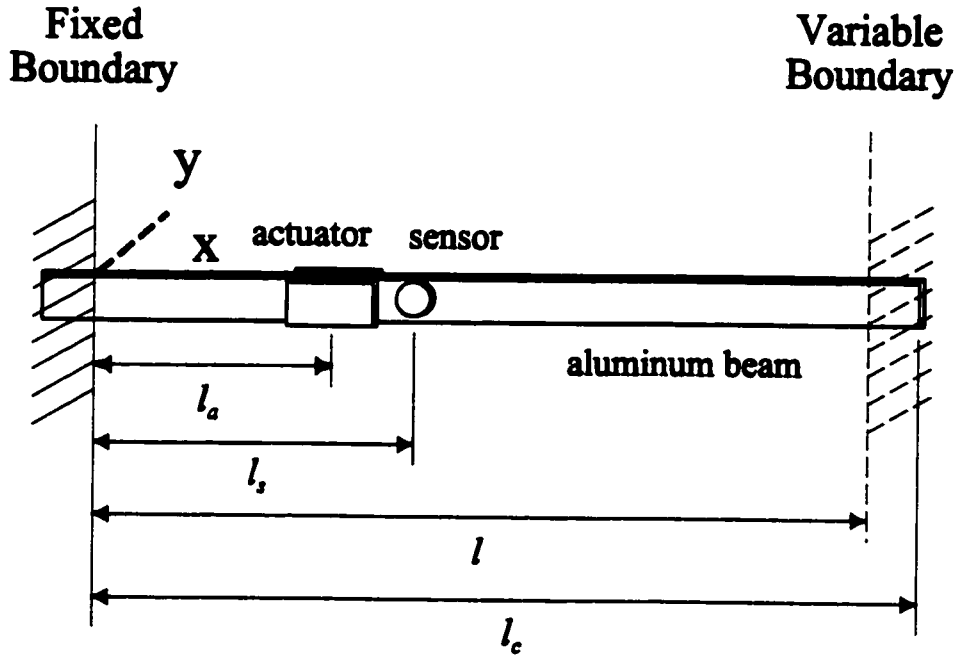

Figure 3.2: Beam dimensions.

Its geometric and material characteristics are given in Table 3.1.

Table 3.1: Beam Characteristics

Effective Dimensions [m]		Properties	
length l	0.4960	density ρ	2750 kg/m^3
length l_c	0.5465	elastic modulus E	71.5 GPa
width w	0.02534	shear modulus G	26 GPa
thickness t_b	0.9398 E-3	moment of inertia* I	1.75 E-12 m^4
		cross-sectional area A	23.8 E-6 m^2

*of cross-sectional area about neutral axis of the beam

The actuator and sensor were placed geometrically as close together as possible, and are located at positions $l_a = 0.127\,m$ and $l_s = 0.189\,m$, respectively, along the beam from its permanently fixed end. The characteristics of the actuator and sensor will be given in Chapter 5.

3.4 Beam Model

3.4.1 Selection of Beam Model

The primary mode of vibration utilised in the proposed damage detection approach is that of flexural (or transverse) vibration. In selecting an analytical model of the transverse vibration $y(x,t)$ of the beam, two models were considered:

Euler-Bernoulli (Thin Beam) Model (Gorman 1975)

- rotary inertia and shear deformation are neglected

$$\frac{EI}{\rho A}\frac{\partial^4 y(x,t)}{\partial x^4} + \frac{\partial^2 y(x,t)}{\partial t^2} = \frac{f(x,t)}{\rho A} \tag{3.1}$$

where

E = Young's elastic modulus [N/m^2]

I = cross-sectional area moment of inertia about neutral axis of the beam [m^4]

ρ = density [kg/m^3]

A = cross-sectional area [m^2]

$f(x,t)$ = distributed force per unit length [N/m]

Timoshenko (Thick Beam) Model (Timoshenko et al. 1974)

- rotary inertia and shear deformation are considered

$$\frac{EI}{\rho A}\frac{\partial^4 y(x,t)}{\partial x^4} + \frac{\partial^2 y(x,t)}{\partial t^2} - \frac{I}{A}\left(1+\frac{E}{kG}\right)\frac{\partial^4 y(x,t)}{\partial x^2 \partial t^2} + \frac{\rho I}{kGA}\frac{\partial^4 y(x,t)}{\partial t^4} + \frac{EI}{\rho k A^2 G}\frac{\partial^2 f(x,t)}{\partial x^2} - \frac{I}{kA^2 G}\frac{\partial^2 f(x,t)}{\partial t^2} = \frac{f(x,t)}{\rho A} \tag{3.2}$$

where

k = Timoshenko shear coefficient = 5/6 for beams having a rectangular cross-section

G = shear modulus of the beam [N/m^2]

and

$\rho I / kGA = 1 / \omega_c^2$ where ω_c is a cutoff frequency corresponding to very high order modes at

which the distances between adjacent nodes of vibration become very small yielding shear modes of vibration (Graff 1975). The Euler-Bernoulli model becomes increasingly less valid as the frequencies of the dominant mode shapes approach this cutoff value.

Upon inspection of Equations (3.1) and (3.2), it is seen that the three terms which comprise the Euler-Bernoulli governing equation are all found within the Timoshenko equation. Using the beam characteristics listed in Table 3.1, the constant coefficients of each term in Equation (3.2) were calculated and are given in Table 3.2 below:

Table 3.2: Numerical Values of Timoshenko Equation Coefficients

Equation Term Number	Coefficient	Value
1	$EI / \rho A$	1.912 m^4/s^2
2	1	1
3	$-(I/A)(1+E/kG)$	-3.16E-7 m^2
4	$\rho I / kGA$	9.33E-15 s^2
5	$EI / \rho kA^2G$	3.71E-6 m^3/kg
6	$-I / kA^2G$	1.426E-13 m^2/N
7	$1 / \rho A$	15.28 m/kg

The simpler Euler-Bernoulli model can be used for the beam having the characteristics listed in Table 3.1 for the following reasons (Iong 1997):

- the beam is very thin (length-to-thickness ratio of 580) and, as such, effects of rotary inertia

and shear deformation are minimal;

- the excitation frequencies used for the numerical simulations (Chapter 4) and experimental results (Chapter 5) are several orders of magnitude lower than the cutoff frequency (ω_c = 10.35 Mrad/s or 1.648 MHz) of the beam;
- the magnitude of the coefficients not common between the two models are much smaller than those which are common (Table 3.2).

3.4.2 Euler-Bernoulli Beam Model

The model presented in this section can be found in (Necsulescu 1996; Necsulescu and DeAbreu 1998; Necsulescu et al. 1998). See also (Iong 1997).

The Euler-Bernoulli model can be expressed as

$$\ddot{y}(x,t) + a^2 y''''(x,t) = \frac{f(x,t)}{\rho A} \tag{3.3}$$

where

$$\ddot{y}(x,t) = \frac{\partial^2 y(x,t)}{\partial t^2} \qquad \text{and} \qquad y''''(x,t) = \frac{\partial^4 y(x,t)}{\partial x^4}$$

and

$$a = \sqrt{\frac{E I}{\rho A}}$$

and all other constants are defined in Sec. 3.4.1.

For solving a fourth order partial differential Euler-Bernoulli equation, four boundary conditions and two initial conditions are needed. For initial conditions, in both cases the beam is assumed initially at rest:

$$y(x,0) = 0 \qquad \textit{and} \qquad \dot{y}(x,0) = 0$$

The boundary conditions for the fixed-fixed case are zero deflection and zero slope at both ends of the beam, and for the cantilever case are zero deflection and zero slope at fixed end of the beam and zero shear and zero moment at the free end (Table 3.3):

Table 3.3: Boundary Conditions of the Beam

Fixed-Fixed	Cantilever
$y(0,t) = 0$	$y(0,t) = 0$
$y'(0,t) = 0$	$y'(0,t) = 0$
$y(l,t) = 0$	$y''(l_c,t) = 0$
$y'(l,t) = 0$	$y'''(l_c,t) = 0$

The distributed vertical force $f(x,t)$, produces a vertical acceleration excitation, $f(x,t)/\rho A$ [m/s^2]. The bending moment produced by the piezoceramic actuator is modelled as the resulting transverse acceleration excitation $a(t)$, concentrated at the centre-point of the actuator ($x = l_a$).

$$\frac{f(x,t)}{\rho A} = a(t)\,\delta(x - l_a) \tag{3.4}$$

where the Dirac delta function gives

$$\delta(x - l_a) = \begin{cases} \infty \text{ (and area of unity)} & \text{for } x = l_a \\ 0 & \text{elsewhere.} \end{cases} \tag{3.5}$$

The acceleration excitation is a sinusoidal signal of magnitude α [m/ s^2] and frequency Ω [rad/s]

$$a(t) = \alpha \sin \Omega t \tag{3.6}$$

The response $y(x,t)$ to the beam excitation is assumed to be measured by a sensor which is located at $x = l_s$

$$y(l_s,t) = y(x,t)\Big|_{x = l_s} \tag{3.7}$$

The analytical solutions for the two cases defined in Sec. 3.2 can be obtained by calculating first the spatial solution (Inman 1994) using the separation of variables $y(x,t) = X(x)\,T(t)$

$$\ddot{T}_n(t)\,X_n(x) + a^2\,T_n(t)\,X_n''''(x) = \frac{f(x,t)}{\rho A} \tag{3.8}$$

where subscript n refers to the n^{th} natural frequency obtained from the homogeneous Euler-Bernoulli equation

$$\ddot{T}_n(t)\, X_n(x) + a^2\, T_n(t)\, X_n''''(x) = 0 \tag{3.9}$$

By rearranging Eq. (3.9),

$$\frac{\ddot{T}_n(t)}{T_n(t)} = -a^2 \frac{X_n''''(x)}{X_n(x)} = -\omega_n^2 \tag{3.10}$$

where ω_n is the n^{th} natural frequency of the beam, the homogeneous spatial equation then becomes

$$X_n''''(x) - \left(\frac{\omega_n}{a}\right)^2 X_n(x) = 0 \tag{3.11}$$

and, for the boundary conditions in Table 3.3, it has the following solutions of the n^{th} mode shape:

$$X_n(x) = B_n \left[A_n (\sinh \beta_n x - \sin \beta_n x) - \cosh \beta_n x + \cos \beta_n x\right] \tag{3.12}$$

where

$$A_n = \frac{\cosh \beta_n l - \cos \beta_n l}{\sinh \beta_n l - \sin \beta_n l} \quad \textit{(fixed-fixed beam of length } l\textit{)}$$

$$A_n = \frac{\sinh \beta_n l_c - \sin \beta_n l_c}{\cosh \beta_n l_c + \cos \beta_n l_c} \quad \textit{(cantilever beam of length } l_c\textit{)}$$

where B_n is an arbitrary coefficient, and the wave number β_n can be expressed in terms of the natural frequency and the coefficient a as $\beta_n^2 = \omega_n / a$. Its n^{th} value is found as the n^{th} root of the following

equations:

$$\cosh \beta_n l \cos \beta_n l = 1 \quad \textit{(fixed-fixed beam of length } l\textit{)} \tag{3.13}$$

$$\cosh \beta_n l_c \cos \beta_n l_c = -1 \quad \textit{(cantilever beam of length } l_c\textit{)} \tag{3.14}$$

Then, the n^{th} natural frequency of the beam can be expressed as

$$\omega_n = \beta_n^2 a \tag{3.15}$$

or

$$\omega_n = (\beta_n L)^2 \sqrt{\frac{E I}{\rho A L^4}} \tag{3.16}$$

where L is either l or l_c.

Applying Laplace transform with respect to t to the non-homogeneous Euler-Bernoulli beam equation gives, for zero initial conditions (beam initially at rest),

$$s^2 y(x,s) + a^2 y''''(x,s) = \frac{f(x,s)}{\rho A} \tag{3.17}$$

Applying the expansion in a series of normal modes (Graff 1975), it is assumed

$$y(x,s) = \sum_{n=1}^{\infty} a_n(s)\, X_n(x)$$
$$f(x,s) = \sum_{n=1}^{\infty} b_n(s)\, X_n(x) \qquad (3.18)$$

where

$$b_n(s) = (2/L) \int_0^L f(x,s) X_n(x)\, dx$$

and, using the non-homogeneous spatial equation (Graff 1975), obtained for $T(t) = e^{-i\omega t}$ and $f(x,t) = F(x)e^{-i\omega t}$,

$$a_n(s) = \frac{b_n(s)}{A\rho(a^2\beta_n^4 + s^2)}$$

This gives

$$y(x,s) = \frac{2}{A\rho L} \sum_{n=1}^{\infty} \frac{X_n(x)}{a^2\beta_n^4 + s^2} \int_0^L f(U,s) X_n(U)\, dU \qquad (3.19)$$

The solutions $y(x,s)$ for Euler-Bernoulli beam are then obtained using convolution theorem.

Assuming a concentrated (at $x = l_a$) sinusoidal short duration acceleration excitation applied at $t = 0$ and removed at $t = t_{ex}$,

$$f(x,t) = \alpha \sin\Omega t \, \delta(x - l_a) \, [u(t) - u(t - t_{ex})] \, \rho A \tag{3.20}$$

where $u(t)$ is the unit step function. The transverse displacement $y(x,t)$ of the beam is derived by integrations with respect to U and T in Equation (3.19) expression for the derived mode shapes $X_n(x)$ for the two limiting boundary condition cases of the beam.

The following expression is obtained as the solution:

$$y(x,t) = \frac{2\alpha}{L} \sum_{n=1}^{\infty} \frac{X_n(l_a) \, X_n(x) \, T_n(t)}{\omega_n \, (\omega_n^2 - \Omega^2)} \tag{3.21}$$

where

$$T_n(t) = \omega_n [\sin\Omega t_{ex} \cos\omega_n (t - t_{ex})] + \Omega [\cos\Omega t_{ex} \sin\omega_n (t - t_{ex}) - \sin\omega_n t]$$

Equation (3.21) gives the transverse displacement of the beam at any position x along the beam at any time t. Since only one sensor is present on the beam (located at $x = l_s$), the model, used for the numerical simulations presented in the next chapter, becomes

$$y(l_s,t) = \frac{2\alpha}{L} \sum_{n=1}^{\infty} \frac{X_n(l_a) \, X_n(l_s) \, T_n(t)}{\omega_n \, (\omega_n^2 - \Omega^2)} \tag{3.22}$$

3.5 Piezoelectric Element Models

3.5.1 Piezoelectric Behaviour

The linearized constitutive relations describing piezoelectric behaviour are given below (Standards Committee of the IEEE Ultrasonics, Ferroelectrics, and Frequency Control Society 1987; Goldfarb and Celanovic 1996):

$$\boldsymbol{S} = \boldsymbol{s}^{\boldsymbol{E}}\boldsymbol{T} + \boldsymbol{d}\boldsymbol{E} \tag{3.23}$$

$$\boldsymbol{D} = \boldsymbol{d}\boldsymbol{T} + \boldsymbol{\epsilon}^{\boldsymbol{T}}\boldsymbol{E} \tag{3.24}$$

where

$\boldsymbol{S}$ = strain tensor [m/m]

$\boldsymbol{s}^{\boldsymbol{E}}$ = compliance matrix in the presence of a constant electric field [m^2/N]

$\boldsymbol{T}$ = stress tensor [N/m^2]

$\boldsymbol{d}$ = matrix of piezoelectric charge constants [C/N] or [m/V]

$\boldsymbol{E}$ = electric field vector [V/m]

$\boldsymbol{D}$ = the electric displacement vector [V/m^2]

$\boldsymbol{\epsilon}$ = dielectric permittivity constant matrix measured at constant stress [F/m]

The terms of the piezoelectric constant matrix $\boldsymbol{d}$ contains charge constants d_{ij} where

$$d_{ij} = \frac{charge\ produced\ in\ direction\ i}{force\ applied\ in\ direction\ j} \tag{3.25}$$

where the first subscript i indicates the poling direction of the sensor (i.e., the direction perpendicular to the electrodes) and the second subscript j indicates the direction of the applied stress (i.e., deformation). Another related piezoelectric coefficient is the voltage constant g_{ij}:

$$g_{ij} = \frac{field\ produced\ in\ direction\ i}{stress\ applied\ in\ direction\ j} \left[\frac{Vm}{N}\right] \tag{3.26}$$

where the subscripts retain the same meaning as before. The two constants are related to each other through the dielectric permittivity as

$$d_{ij} = \epsilon g_{ij} \tag{3.27}$$

3.5.2 Sensor Model of a Piezoelectric Element

A simple example will be used to derive a relationship that can be applied when measuring the deflection of a unsecured or free-standing rectangular plate piezoelectric element (Fig. 3.3).

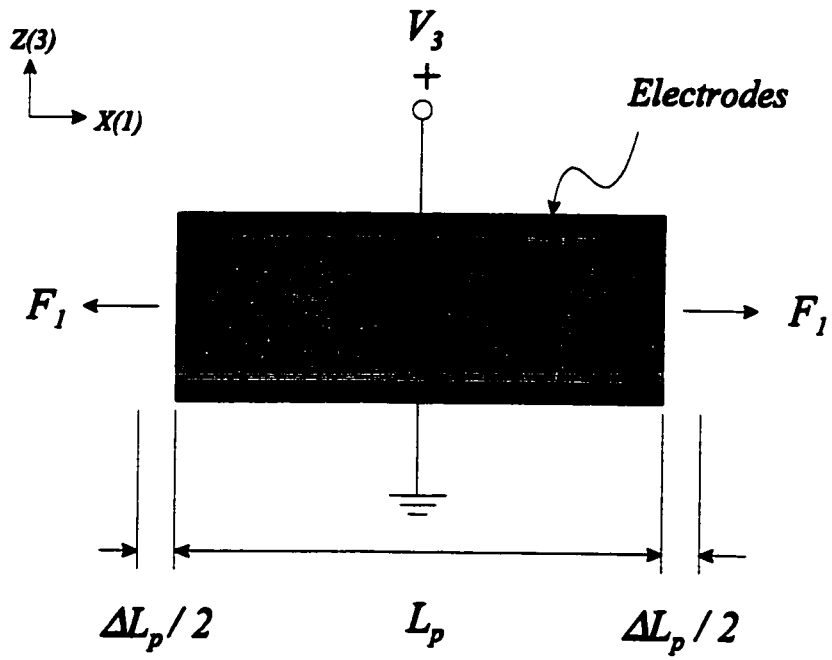

Figure 3.3: Piezoelectric element.

The element is of length L_p and width W_p, and has poles across its thickness t_p. If an external force F_1 is applied longitudinally to both ends of the element, a corresponding longitudinal stress σ_1 and a charge density D_3 results. In the absence of an external electric field, these two quantities are related in Eq. (3.24) through the longitudinal charge constant d_{31} of the sensor as

$$D_3 = d_{31}\,\sigma_1 \tag{3.28}$$

where

$$D_3 = -\frac{Q}{L_p W_p} \qquad \textit{and} \qquad \sigma_1 = E\frac{\Delta L_p}{L_p} = \frac{1}{s_{11}^E}\frac{\Delta L_p}{L_p} \tag{3.29}$$

where Q is the generated charge, E is the elastic modulus and s_{11}^{E} is the compliance (both in the longitudinal direction), and ΔL_p is the longitudinal deflection of the element. The charge Q can be expressed as

$$Q = CV_3 = \frac{\epsilon W_p L_p}{t_p} V_3 \tag{3.30}$$

where C is the capacitance of the element, ϵ is its dielectric constant and, assuming an infinite impedance measurement system is used, V_3 is the measured voltage across the thickness t_p of the element. Thus, combining the above equations, the deflection-voltage relationship can be expressed as

$$\Delta L_p = K_L V_3 \tag{3.31}$$

where the constant K_L is given as

$$K_L = -\frac{\epsilon s_{11}^{E}}{d_{31}} \frac{L_p}{t_p} \tag{3.32}$$

and since the charge coefficient is related to the voltage coefficient as $d_{31} = \epsilon g_{31}$, a simpler expression for the constant K_L is

$$K_L = -\frac{s_{11}^{E}}{g_{31}} \frac{L_p}{t_p} \tag{3.33}$$

A similar relationship can be derived for the deflection of the piezoelement in the thickness (z-)direction due to a force F_3 applied to the element in the z-direction:

$$\Delta t_p = K_t V_3 \tag{3.34}$$

where

$$K_t = \frac{s_{33}^E}{g_{33}} \tag{3.35}$$

3.5.3 Actuator Model of a Piezoelectric Element

The actuator model is based on the constitutive equations of Sec. 3.5.1:

$$\boldsymbol{S} = s^E \boldsymbol{T} + d\boldsymbol{E} \tag{3.23}$$

$$\boldsymbol{D} = d\boldsymbol{T} + \epsilon^T \boldsymbol{E} \tag{3.24}$$

Force results along the longitudinal (x-) direction due to a voltage applied in the thickness (z-) direction.

Chapter 4

Simulation Study

4.1 Introduction

In this chapter, simulation studies, based on the analytical models of Chapter 3, are presented which show that significant differences can be predicted between the transient response of the secure and disconnected cases of the beam. The positive results of the simulation study made it feasible to study, experimentally, intermediate states of joint loosening in the beam connection (Chapter 5). The present chapter begins with a presentation of the calculated natural frequencies of the secure and disconnected cases of the beam. Next, the details of the excitation selection process are discussed. Then, graphic results of the simulation are presented followed by a discussion.

4.2 Calculation of Natural Frequencies

Determination of the natural frequencies of the beam is required for selecting an effective excitation frequency to be used in the proposed approach. The natural frequencies of the beam were numerically determined using an m-file (Appendix C) in MATLAB (Ver. 5) based on the model presented in Chapter 3 (Eqs. (3.13) to (3.16)):

Table 4.1: Calculated Natural Frequencies

	Calculated Natural Frequencies [Hz]									
Number	1	2	3	4	5	6	7	8	9	10
Fixed-Fixed	20	55	108	179	267	373	497	638	797	974
Cantilever	2.6	16	45	89	147	220	307	409	525	656

4.3 Selection of Excitation Characteristics for Simulation Analysis

For the proposed damage detection method to be feasible, detectable differences in the transient response of the damaged beam (including the extreme case of the disconnected beam) and secure beam must be present for the same excitation. Thus, the beam under damage testing is diagnosed using an excitation having a frequency Ω which satisfies two criteria:

- Ω is close in value to one of the higher natural frequencies, corresponding to the secure beam

situation, and for which a large magnitude of response exists;

- Ω is far in value from the two adjacent natural frequencies of the disconnected beam.

Since natural frequencies change with boundary conditions, by using such a frequency for detecting the state of integrity of the boundary, the closer the beam state is to that of the disconnected beam, the greater will be the differences (and therefore more detectable) between the transient responses for the damaged beam and the secure beam. The frequency chosen is 374.5 Hz (2353 rad/s) which is very near to the 6th natural frequency of the secure case but far from both the 7th and 8th frequencies of the disconnected case which are 307 Hz and 409 Hz, respectively (see Table 4.1).

Since the free vibration of a flexible beam is sinusoidal with respect to time t (and position x along the beam), the selection of a sinusoidal waveform for the excitation function is a logical one. Several values for the number of excitation cycles were investigated all yielding similar results from the viewpoint of damage detection. The simulations given in this chapter were based on fifty (50) excitation cycles since the experimental study was also based on this value. Justification for using this value is given in Chapter 5. The amplitude α of the excitation was simply chosen as unity given the purpose of the analytical study (Sec. 3.1). The excitation characteristics are given in Table 4.2.

Table 4.2: Excitation Characteristics for Simulation Study

Wave Type	Frequency [Hz]	Number of Cycles	Alpha [m/s^2]
sinusoidal	374.5*	50	1

* The frequency was chosen to be near to the 6th natural frequency of the secure beam.

4.4 Numerical Calculation of the Transient Response of the Beam to Sinusoidal Transverse Excitation

The simulated responses of the beam for the two extreme cases of joint loosening were numerically determined using an m-file in MATLAB (Ver. 5) based on the model presented in Chapter 3 (Eq. (3.22)). The m-file program used to perform the calculation is given in Appendix C. A simplified flow chart of the program is given in Figure 4.1. Each solution value $y(l_s,t_i)$ is calculated to an precision of 0.01% or better. N is the total number of discrete time samples comprising the response; it corresponds to a total response time of 0.8 seconds for a sampling frequency of 5992 Hz (or sampling time of 0.167 milliseconds). The specified value for the sampling frequency was chosen such that exactly 16 samples were taken per excitation cycle (i.e., 374.5 excitation cycles/second X 16 samples/excitation cycle = 5992 samples/second).

The simulated responses of the secure and disconnected case are displayed in Figures 4.2 and 4.3, respectively. The vertical dashed line, located at time t = 0.13 seconds, indicates the time at which the applied excitation to the beam is removed.

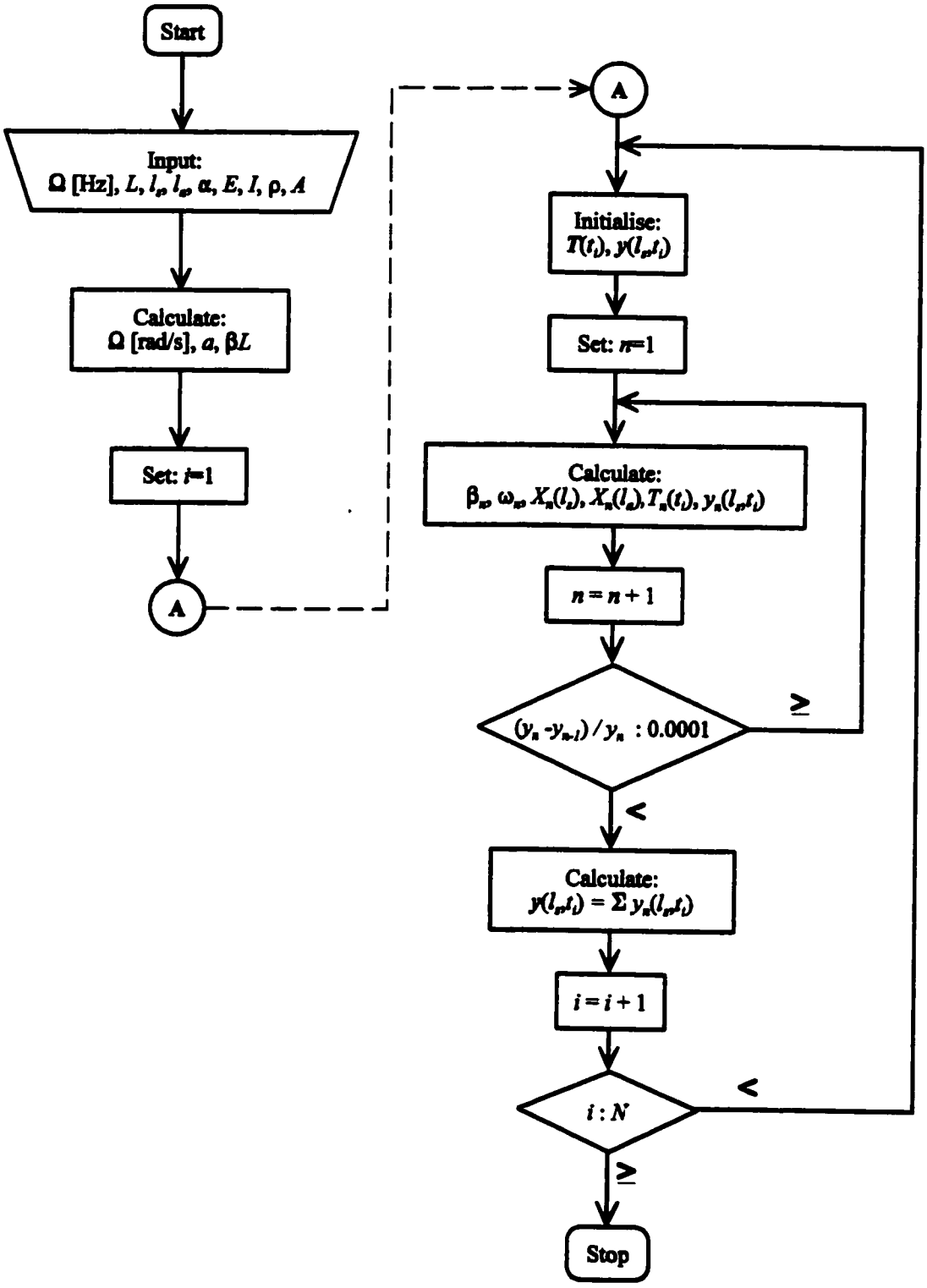

Figure 4.1: Simple flow chart of simulation program used to determine the transient response of the beam.

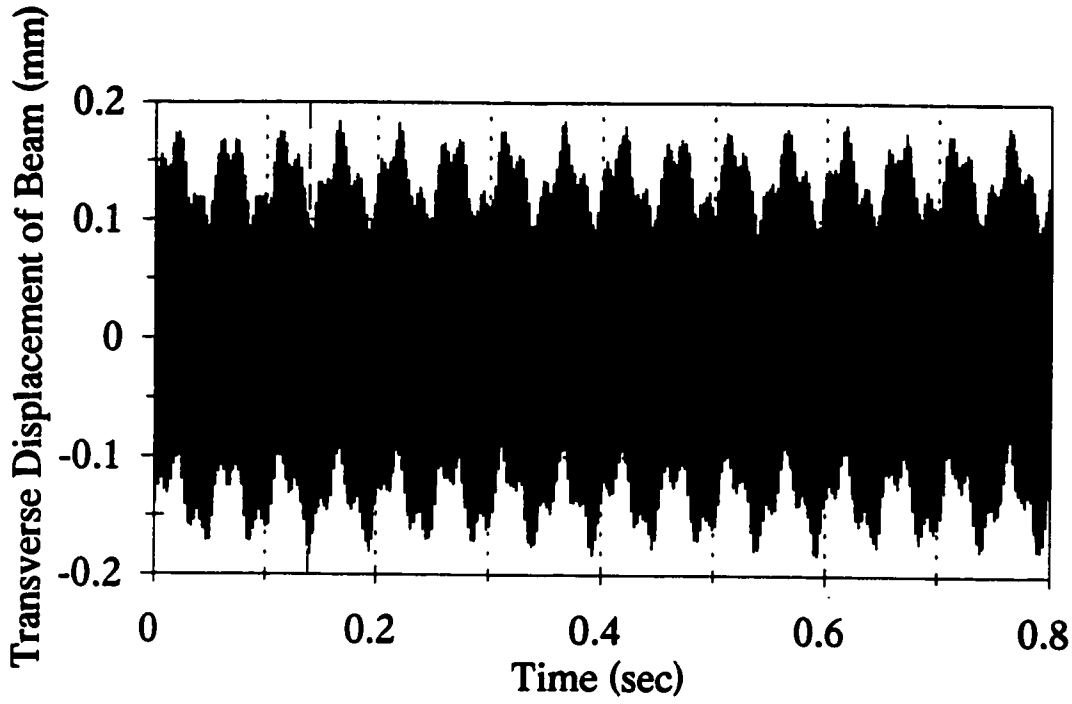

Figure 4.2: Simulated transient response of the secure beam.

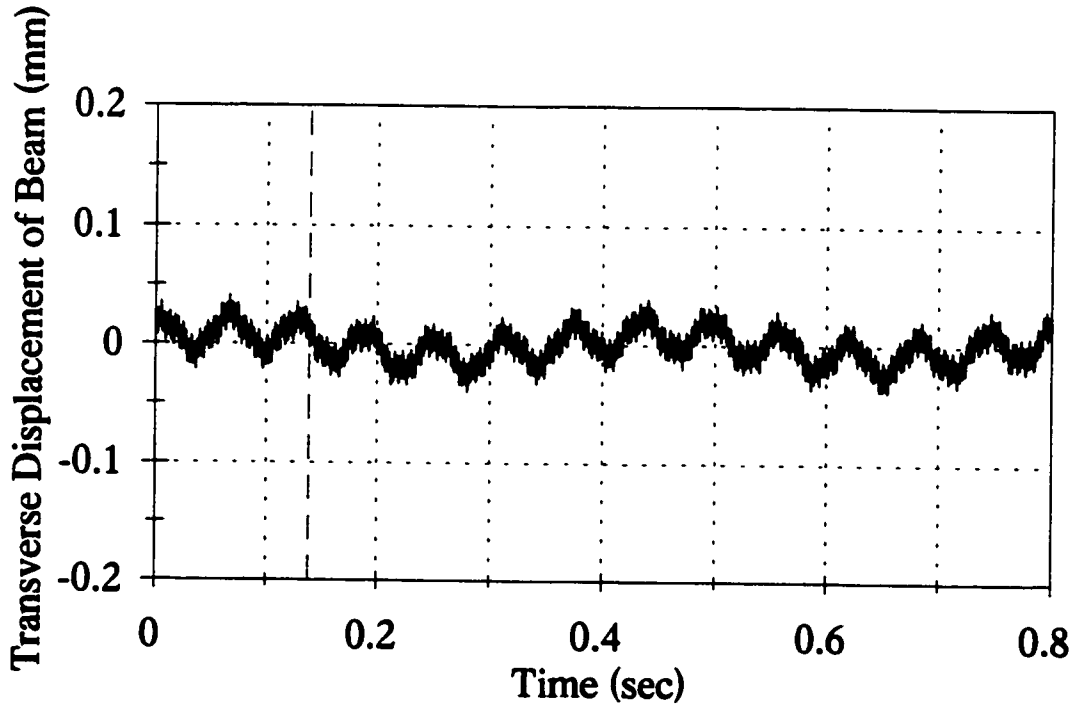

Figure 4.3: Simulated transient response of the disconnected beam.

4.5 Discussion of Results

The responses of both the secure and disconnected beam cases contain several natural frequencies, three being more significant than the others in terms of amplitude of response. In the secure case, the response contains mainly the 1st , 2nd and 6th fixed-fixed beam natural frequencies with the 6th frequency being the most dominant in terms of amplitude of response. This is expected since the beam was excited at a frequency very near in value to the 6th natural frequency. For the disconnected case, the response contains mainly the 1st, 2nd, and 8th natural frequencies of the cantilever beam with the 1st and 2nd frequencies being dominant.

The beam response of secure case differs from that of disconnected case in two important ways:

- the maximum amplitude of the transient section of the response in secure case is about four times larger than that of the disconnected case;
- the ratios of the individual response amplitudes of the three dominant frequencies are significantly different in the two cases. (i.e., in the response of the secure case (Fig. 4.2), the response amplitude of the natural frequency (6th) closest to the excitation frequency is significantly greater than those of the other two frequencies present in the response; whereas, in the response of the disconnected case (Fig. 4.3), the response amplitude of the natural frequency (8th) closest to the excitation frequency is actually lower in magnitude than that of the other two frequencies present in the response.

Since a significant measurable difference was found between the respective transient responses of the secure and disconnected beam cases, the proposed approach was extended to intermediate damage cases (Chapter 5). No damping is represented in the analytical model and, as a result, its effect cannot be evaluated. Experimental study permits to overcome this limitation.

Chapter 5

Experimental Study

5.1 Experimental Set-up

The experimental set-up is shown in Figures 5.1 and 5.2. It consists of a flexible aluminum beam (characteristics listed in Sec. 3.3) equipped with a piezo-actuator and a piezo-sensor, two heavy supports for clamping, and the following electronic equipment: PC, power signal generator, oscilloscope, 2nd-order analog filter and dSPACE digital signal processor (DSP). Experiment testing, generation of excitation signal and measurement of response signal are controlled using the DSP software and a C-program (Appendix D). The clamping force is modified by the tightening of two bolts onto a number of Belleville washers to secure the end of the beam between a mounting plate and the side of the heavy support at the variable boundary.

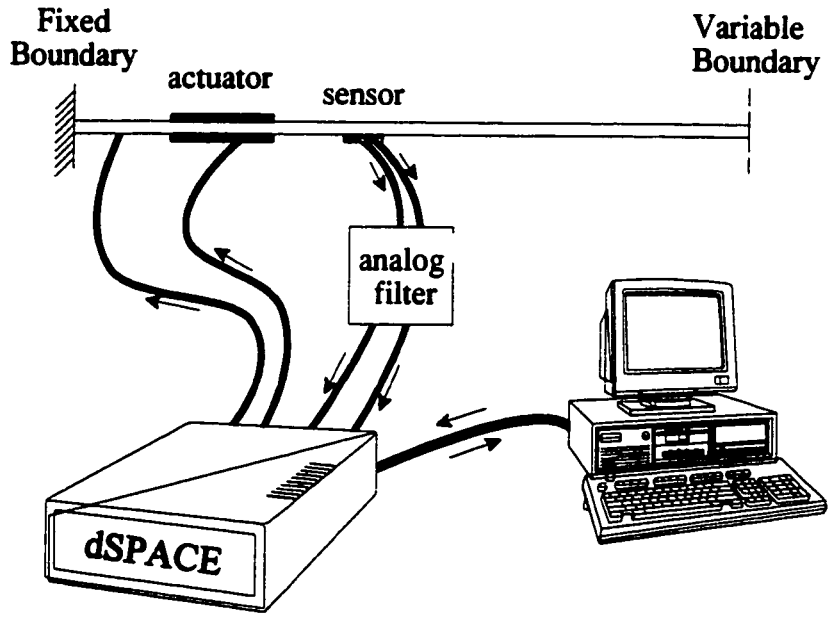

Figure 5.1: Experimental set-up.

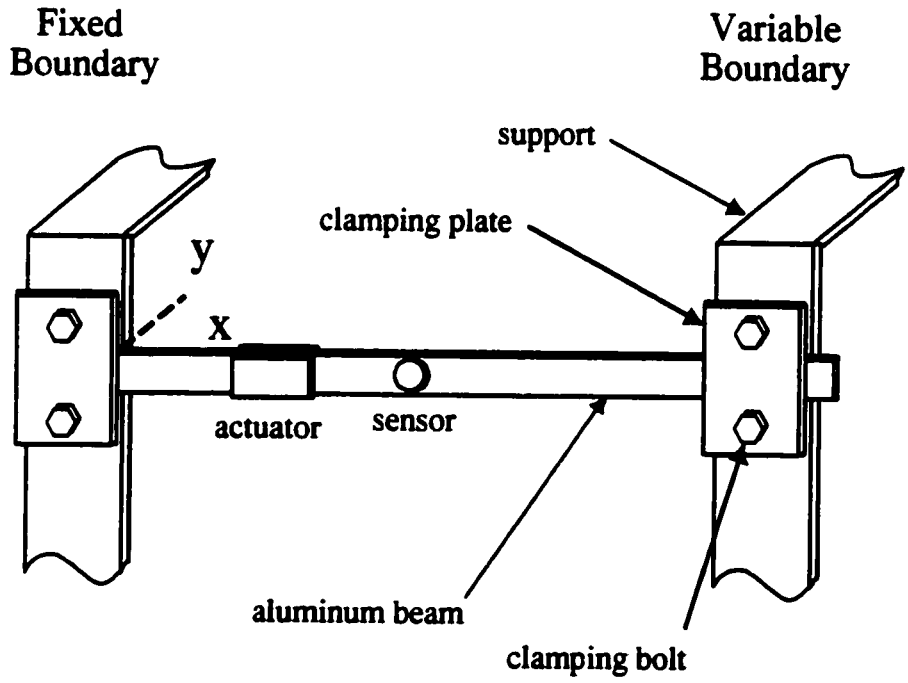

Figure 5.2: Clamping of the beam.

5.1.1 Experimental Equipment Description

Actuator and Sensor

The actuator is composed of eight 0.5" X 1.5" X 0.020" (12.7mm X 38.1mm X 0.5mm) BM400 Type I Sensor Technology (Prasad 1995) rectangular piezoceramic elements, four on either side of the beam. Therefore, the length L_a of the actuator is 76.2 mm, its width w_a and its effective thickness t_a is 1.0 mm. It was desirable to use a distributed actuator whose length is similar in magnitude to the inter-nodal distance of the excited mode shape (6^{th}). The sensor is a BM400 Type I Sensor Technology circular piezoceramic element 20.0 mm in diameter and 1.0 mm in thickness. The characteristics of both the sensor and the actuator are summarised in Table 5.1:

Table 5.1: Actuator and Sensor Characteristics

Effective Dimensions [m]				Properties	
Actuator		Sensor			
length L_a	0.0762	diameter D_s	0.0200	charge constant g_{31}	-10.5 X 10^{-3} Vm/N
width w_a	0.0254	thickness t_s	0.0010	compliance s_{11}^E	12.5 X 10^{-12} m^2/N
thickness t_a	0.0010				

dSPACE Digital Signal Processor (DSP)

dSPACE (dSPACE 1990) hardware was used to physically generate the sinusoidal excitation voltage signal sent to the piezo-actuator and to physically measure the corresponding beam response voltage signal generated at the piezo-sensor. Three boards are utilised: DS1002 processor board, DS2101

digital-to-analog conversion (DAC) and DS2001 analog-to-digital conversion (ADC) boards. The DS1002 processor board utilises a TMS320C30 digital signal processor to execute monitor program commands.

The following DSP software is used:

- SED30 - setup editor utility program used to create and edit setup files which in turn are used to configure the various boards mentioned previously
- MON30 - monitor utility program used to load, evaluate and execute the system setup files and DSP object code modules (e.g., C-program in Appendix D)
- TRACE30 - module used to record and graphically display all signals and parameters present in the processor memory of the DS1002 board

Oscilloscope

Brüel & Kjel Precision (Model No. 2522) 20 MHz digital storage oscilloscope was used in measuring the natural frequencies of the beam and in verifying the measured experiment results of the dSPACE TRACE30.

Signal Generator

Brüel & Kjel Precision (Model No. 3022) signal generator was used in conjunction with the oscilloscope for measuring the natural frequencies of the beam.

2nd-order Low Pass Analog Filter

The filter was designed based on the equal-component-value Sallen-Key circuit model (Lancaster 1996) and was built using capacitors, resistors and an LM741operational amplifier. It has a corner frequency of 884 Hz and no overshoot in its frequency response.

C-Program

The C-program used to control the measurement procedure is listed in Appendix D.

5.1.2 Modification of Clamping Force. Definition of Clamping Force Index

The flexible beam is mounted securely onto the supports by tightening the clamps onto it. The clamping force F_c exerted by the variable boundary clamp on the beam can be modified by loosening or tightening the clamp bolts. The secure case clamping force corresponds to a bolt torque of approximately 2.5 foot-lb (3.4 N-m) which is the precision of the torque wrench used for measurement. The disconnected case corresponds to a bolt torque of zero. However, because of the low torques involved, the clamping forces of the intermediate damaged cases could not be quantified in terms of bolt torque. They can only be quantified in terms of tightening rotations of the clamp bolts - the more rotations of the bolt the higher the clamping force. This allows for only a simple relative discernment of the different damaged cases since bolt turns cannot be correlated with clamping force as easily as that of bolt torque. Therefore, a clamping force index i is used to indicate the relative degree of the clamping force. The higher the index value is, the larger the clamping force and therefore the more secure is the connection. The index ranges from one (disconnected case) to

seven (secure case).

5.2 Experimental Determination of Natural Frequencies

The natural frequencies of the actual beam were determined experimentally for the two extreme boundary condition cases and are given below in Table 5.2:

Table 5.2: Natural Frequencies of the Beam Obtained from Experiment

	Experimental Natural Frequencies (Hz)									
Number	1	2	3	4	5	6	7	8	9	10
Fixed-Fixed	17.5	52	104	149	266	361	512	595	796	979
Cantilever	----	14.5	42.5	87.5	139	215	310	418	534	655

By comparing the values of the calculated (Sec. 4.2) and experimentally determined natural frequencies, it can be seen that most of them agree to within ±8% (excluding the 1st and 4th natural frequencies of the secure beam and the 2nd natural frequency of the disconnected beam) and many of the higher modes agree to within a much lower percentage difference.

5.3 Selection of Excitation Characteristics for Experimental Study

The wave form and frequency of excitation for the experimental study was selected as sinusoidal and 361 Hz (6th natural frequency), respectively, for the same reasons as for the numerical simulations

(Sec. 4.3). The number of cycles in the excitation was chosen as fifty (50) for the following reasons: (1) the amplitude of the response and thus the differences between responses are amplified as the number of excitation cycles is increased (Iong 1997); (2) the range of possible values for the number of excitation cycles is limited by several factors: the size of the DSP buffer (i.e., only 5000 samples could be measured per response), the frequency of excitation and the sampling frequency of the DSP. This value, however, does yield excellent results as will become evident in later sections. The amplitude of the excitation was chosen as 10 V which is the maximum possible for the experimental set-up since no charge amplifier was used. The excitation characteristics are tabulated below:

Table 5.3: Excitation Characteristics for Experimental Study

Wave Type	Frequency [Hz]	No. of Cycles	Volts (max/min)
sinusoidal	361*	50	±10

* The frequency was chosen to be near to the 6th natural frequency of the secure beam.

5.4 Experimental Determination of the Transient Response of the Beam to Sinusoidal Transverse Excitation

The responses of the actual beam for several structural integrity cases ranging from secure to damaged to disconnected were obtained with the experimental set-up described previously and were digitally filtered using an m-file (Appendix C) in MATLAB (Ver. 5). A complete set of filtered and raw (i.e., unfiltered) data plots is given in Appendix A. Three separate measurement trials (A, B and C) were conducted for each damaged case. Selected results are displayed in Figures 5.3 to 5.5. The

damaged cases differ from each other in the amount of force applied by the variable boundary clamp. This is quantified using the clamping force index i explained earlier in Section 5.1.2. As specified earlier for the graphs of the simulated responses of Chapter 4, the dashed line located at time $t = 0.13$ seconds in the following figures indicates the end of the beam excitation phase.

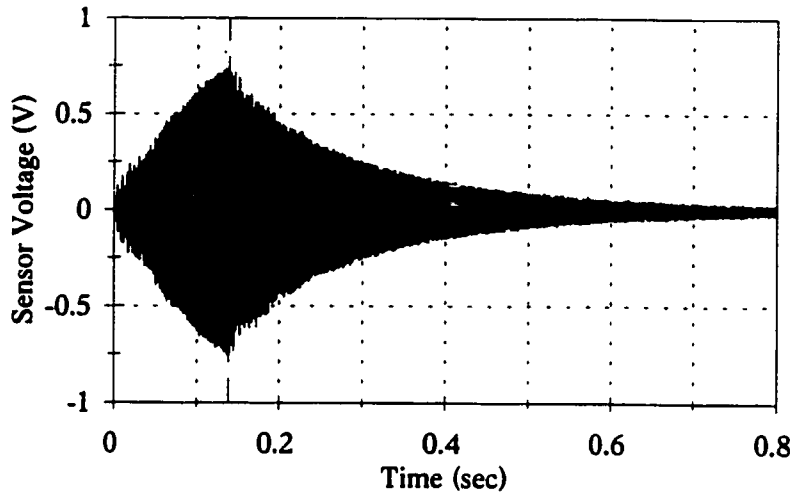

Figure 5.3: Transient response of the secure case of the beam from experiment.

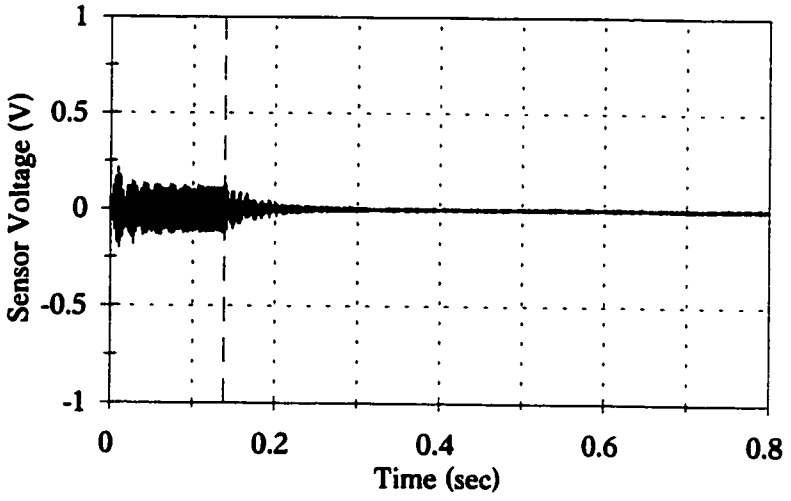

Figure 5.4: Transient response of the disconnected case of the beam from experiment.

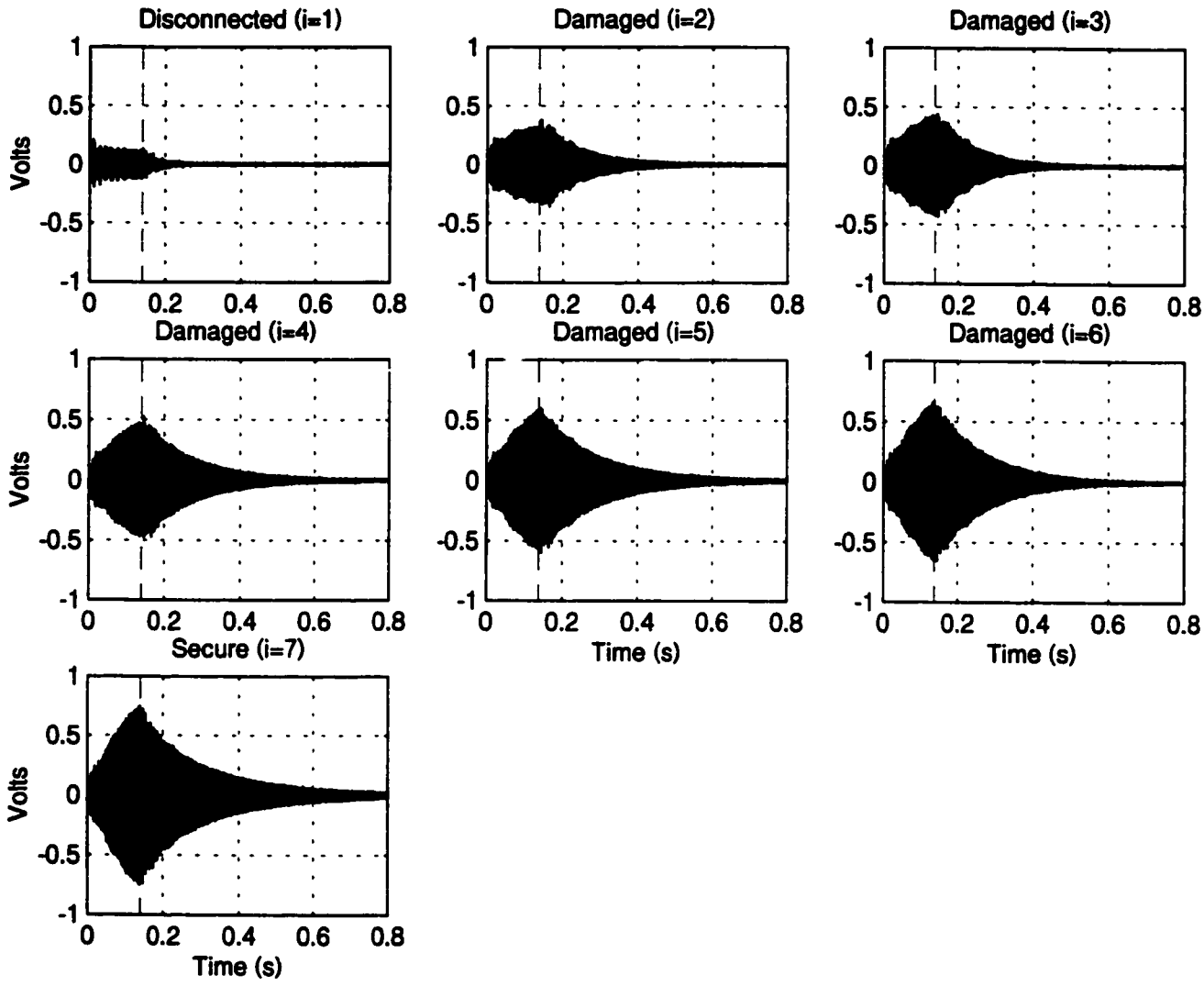

Figure 5.5: Transient responses of all damaged cases of the beam from experiment.

Several points may be made regarding the experimental results for the two limiting cases of joint loosening (Figures 5.3 and 5.4):

- damping is present as can be seen from the gradual increase (in the excitation phase) and the gradual decay (in the non-excitation free vibration phase) of the experimental responses;

- the disconnected case response decays much more quickly with respect to time than the secure case response;

- the maximum amplitude of the secure case response is significantly greater (by a factor of about 3.5) than that of the disconnected case;

- the overall amplitude (i.e., area of the response) of the secure case response is significantly greater than that of the disconnected case.

The latter two observations for the experiment results agree with those found in the corresponding numerical simulations (Figure 4.2 and 4.3). Since the analytical model did not account for structural damping, the former two findings were not observed in simulation.

The following important observation can be made regarding the responses of the practical intermediate damaged cases (Figure 5.5):

- the larger the clamping force, the larger the maximum amplitude of the transient response and the larger the overall amplitude of the response.

The decay duration for the beam response seems to be related to changes in clamping force but further analysis was needed (Chapter 6) to determine the type of relationship.

The monotonical correlation between response amplitude and clamping force (i.e., integrity of the connection) allows for reliable detection of damage (i.e., loosening) in the connection. Response amplitudes close in value to the secure case indicate a more secure connection and amplitudes far in value from the secure case indicate a less secure (i.e., damaged) connection. Using the plots and the abovementioned monotonical relationships, a human operator could determine the state of the structural integrity of the beam connection; however, this is not real-time damage detection. In order to realise real-time detection, differences between various test cases must be quantified in a way that the damage assessment can be performed by a computer-controlled detection system. The analysis presented in the next chapter results in several options for quantifying these differences.

5.5 Repeatability of Measurements

As discussed in Section 5.5, three response trials were recorded for each of the seven damaged cases. The three trials of three separate test cases (secure, disconnected, damaged i=4) are displayed below in Figure 5.6. It is evident from the plots that the measurements were repeatable.

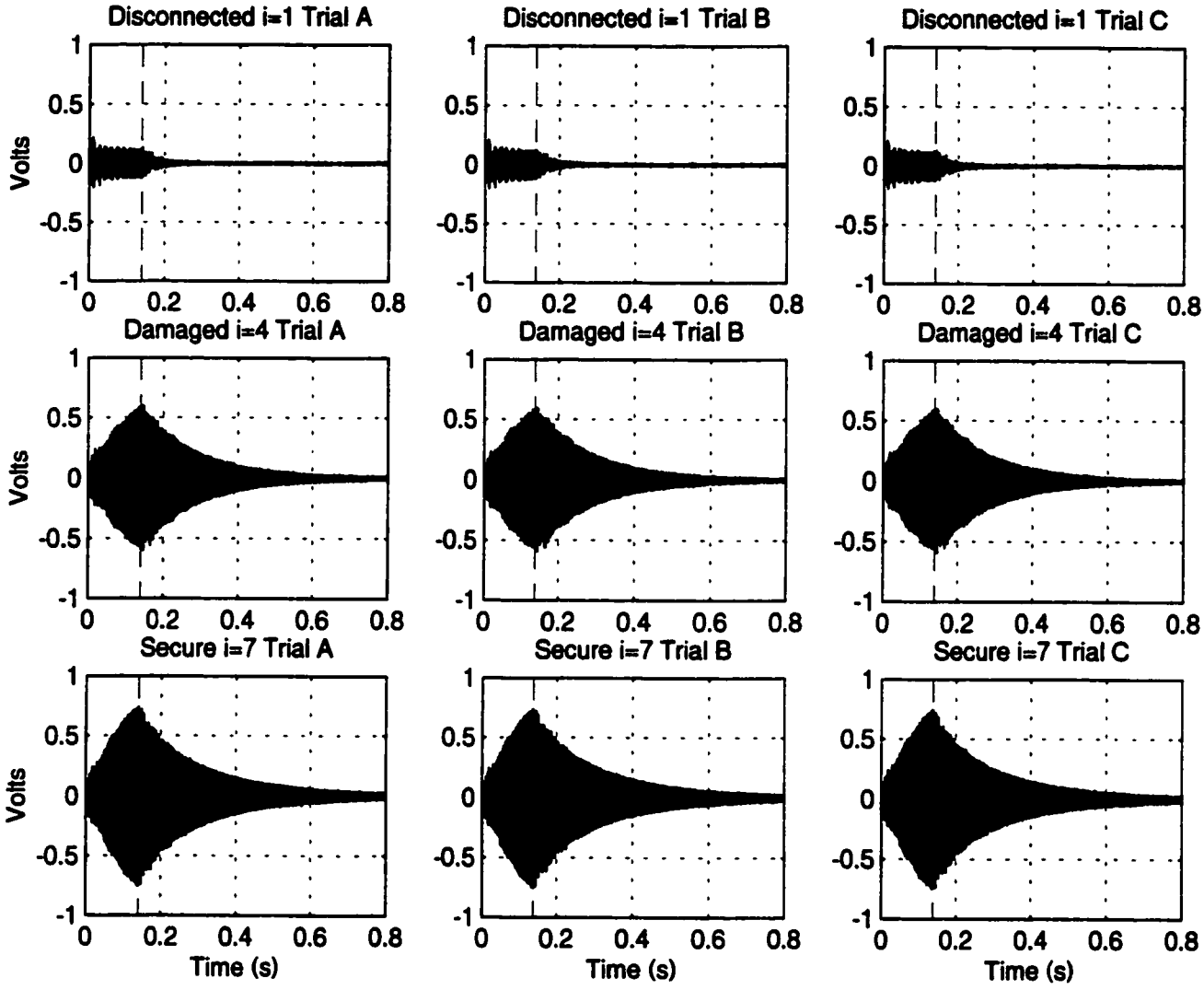

Figure 5.6: Repeated response trials for secure (top three), damaged (middle three) and disconnected (bottom three) cases of the beam.

Chapter 6

Real-Time Damage Detection Approach

6.1 Basic Explanation of the Approach

The proposed approach employs computer analysis of the measured transient response data and quantifies differences between the test case *i* and the secure case of the structure in question (i.e., the flexible beam). In Chapter 5, differences were observed between the secure and damaged cases with respect to three basic characteristics. These included the following: overall response amplitude, maximum amplitude and decay duration. The differences in these three response characteristics are quantified in the present chapter through employment of a damage analysis program (Sec. 6.3.2). The first characteristic, overall response amplitude, is quantified using various damage index equations.

6.2 Damage Index Criteria

For a damage index to be feasible for use in practice, it should satisfy (at a minimum) the following criteria:

- correlate monotonically with the actual damage in the connection (i.e., clamping force F_c);
- require minimal computation because real-life structures contain a large number of flexible components to be diagnosed;
- yield repeatable (i.e., reliable) results.

6.3 Damage Index Analysis

6.3.1 Damage Index Based on Overall Response Amplitude

The three general damage indices tested are overall response amplitude (Type 1), maximum amplitude (Type 2) and decay duration (Type 3). The latter two indices require minimal computation. The first index does, however, involve significant computation and is expressed as the average difference of response amplitudes between the secure case and test case i. For each test case i response, the overall response amplitude index is calculated either using (1) all the response data, or (2) only the maximum and minimum values of each vibration cycle of the response (Figure 6.1).

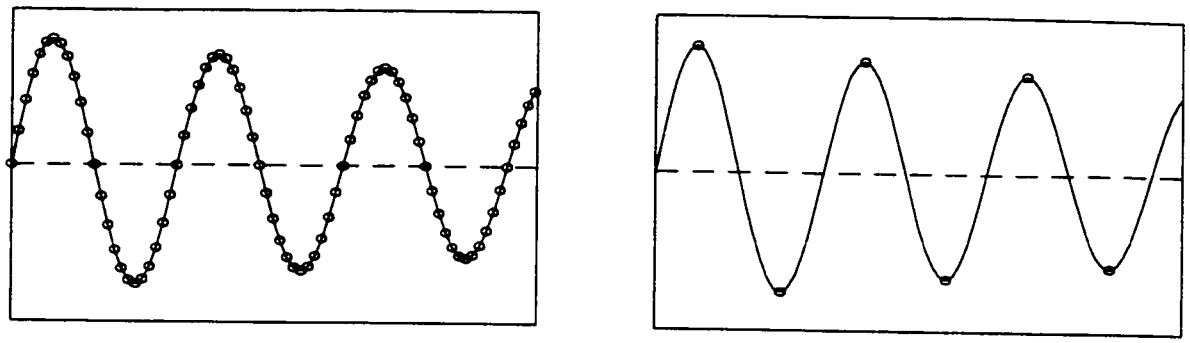

(a) (b)

Figure 6.1: Data samples used for Type 1 (overall response amplitude) damage index calculation - (a) all data samples; (b) only cycle maxima/minima.

In addition, three different time windows are used for calculation of the overall response magnitude damage index (Figure 6.2): (1) the total response - the period of time from the beginning of excitation to the time at which the response amplitude decays to a "cutoff" voltage level of approximately 0.07V; (2) the excitation zone - the period of time from the start of the applied excitation to its removal, and (3) the free vibration zone - the period of time from the removal of the excitation to the time at which the response decays to the 0.07V cutoff level. The cutoff voltage level was chosen to be some value which was greater than the maximum amplitude of the measurement noise (~0.22V) and which yielded satisfactory results. The cutoff voltage level will be discussed further in Section 6.5.

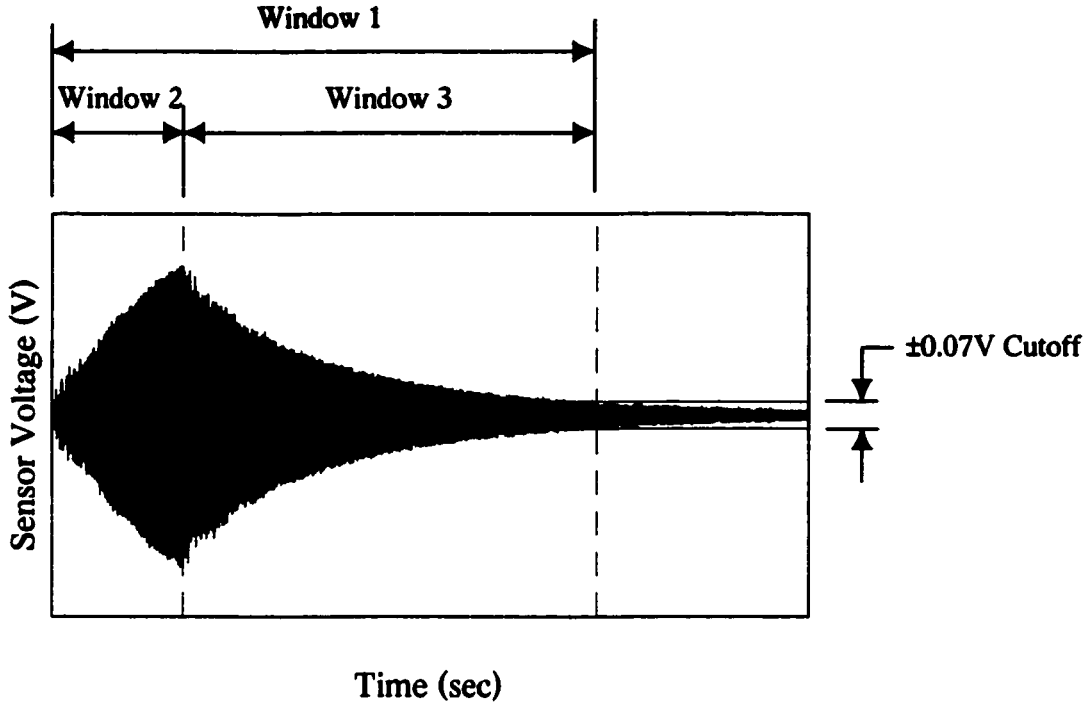

Figure 6.2: Time windows used in calculation of Type 1 damage index.

The various expressions used to quantify differences in the response of the beam are given below:

Damage Index 1 - Difference of the Sums of the Absolute Values of the Samples of the Test Case and Secure Case Responses

$$DI1_i = \frac{\sum_{j=1}^{N_{secure}} \left| V_{secure,j} \right| - \sum_{j=1}^{N_i} \left| V_{i,j} \right|}{N_{secure}} \qquad (6.1)$$

Damage Index 2 - Sum of the Square Roots of the Square of the Difference of the Samples of the Test Case and Secure Case Responses

$$DI2_i = \frac{\sum_{j=1}^{N_i} \sqrt{\left(V_{secure,j} - V_{i,j} \right)^2}}{N_i} \tag{6.2}$$

Damage Index 3 - Sum of the Square Roots of the Square of the Difference of the Absolute Values of the Samples of the Test Case and Secure Case Responses

$$DI3_i = \frac{\sum_{j=1}^{N_i} \sqrt{\left(\left| V_{secure,j} \right| - \left| V_{i,j} \right| \right)^2}}{N_i} \tag{6.3}$$

Damage Index 4 - Square Root of the Sum of the Squares of the Difference of the Samples of the Test Case and Secure Case Responses (Iong 1997)

$$DI4_i = \frac{\sqrt{\sum_{j=1}^{N_i} \left(V_{secure,j} - V_{i,j} \right)^2}}{N_i} \tag{6.4}$$

where V is the sensor voltage, and i is the clamping force index which relates to the magnitude of the clamping force where the number one (1) corresponds to the disconnected case (F_c=0) and the number seven (7) corresponds to the secure case. The index j represents both the response data sample index (for the case in which all response data is used for calculating the damage index) and the response maxima/minima index (for the case in which only the cycle maxima and minima of the response are used in the calculation of index). N is the total number response samples before the response decays to the cutoff voltage level (~0.07V) for the calculation Time Windows 1 and 3, and is the total number of response samples until the end of the excitation period for Time Window 2. The secure case response V_{secure} is the average secure case response and is calculated by averaging sample-by-sample the three responses for the secure case obtained from experiment.

6.3.2 MATLAB Program for Damage Analysis

The process of calculating the various damage indices was performed using an m-file (Appendix C) in MATLAB (Ver. 5). The basic tasks performed by the m-file program are outlined in Table 6.1.

Table 6.1: Tasks Performed by Damage Analysis Program

1	**Input** the experiment parameters, and the experiment response and noise data.
2	**Filter** the response and noise data, digitally.
3	**Calculate,** based on all response data samples, the overall response amplitude (Type 1) damage indices 1 to 4 for all three time windows for each test case *i*.
4	**Graph** the results of all indices calculated in Step 3.
5	**Determine and graph** the cycle maxima and minima for each response.
6	**Calculate,** based on only response maxima and minima, the overall response amplitude (Type 1) damage indices 1 to 4 for all three time windows for each test case *i*.
7	**Graph** the results of all indices calculated in Step 6.
8	**Graph** the maximum amplitude and decay duration indices (Type 2 and 3, respectively).
9	**Output** the numerical results of damage analysis to an ascii file.

6.3.3 Damage Index Results

A complete set of damage index results is given in Appendix B. First considering the Type 1 damage index, which considers overall response magnitude, it was found that all four damage indices yielded results which, in general, satisfied the criteria outlined in Sec. 6.2. The index which best satisfied these criteria, Damage Index 1, is presented here in the main text. The analysis results for Index 1 considering all data samples is displayed in Figure 6.3 for all three time windows. Each of the three bar graphs contains 21 plotted values, three values for each of the seven test cases analysed. The

three values were calculated from the three corresponding responses (ie., Trials A, B and C) measured in experiment for each of the seven clamping force situations. Repeatability (Criterion 3) is important when comparing values within the groups of three, and monotonical relationship to the clamping force index (Criterion 1) is important when comparing one group to another. As explained in Sec. 6.3.1, the clamping force index i ranges from one (disconnected case) to seven (secure case). The analysis results for Index 1 considering only cycle maxima and minima is displayed in Figure 6.4, again for all three time windows.

Results for the maximum response amplitude (Type 2) and decay duration (Type 3) indices are given in Figures 6.5 and 6.6.

In order to ensure the MATLAB program results were correct, an independent calculation was performed using a Quattro Pro spreadsheet. The results of the latter confirmed those of the former.

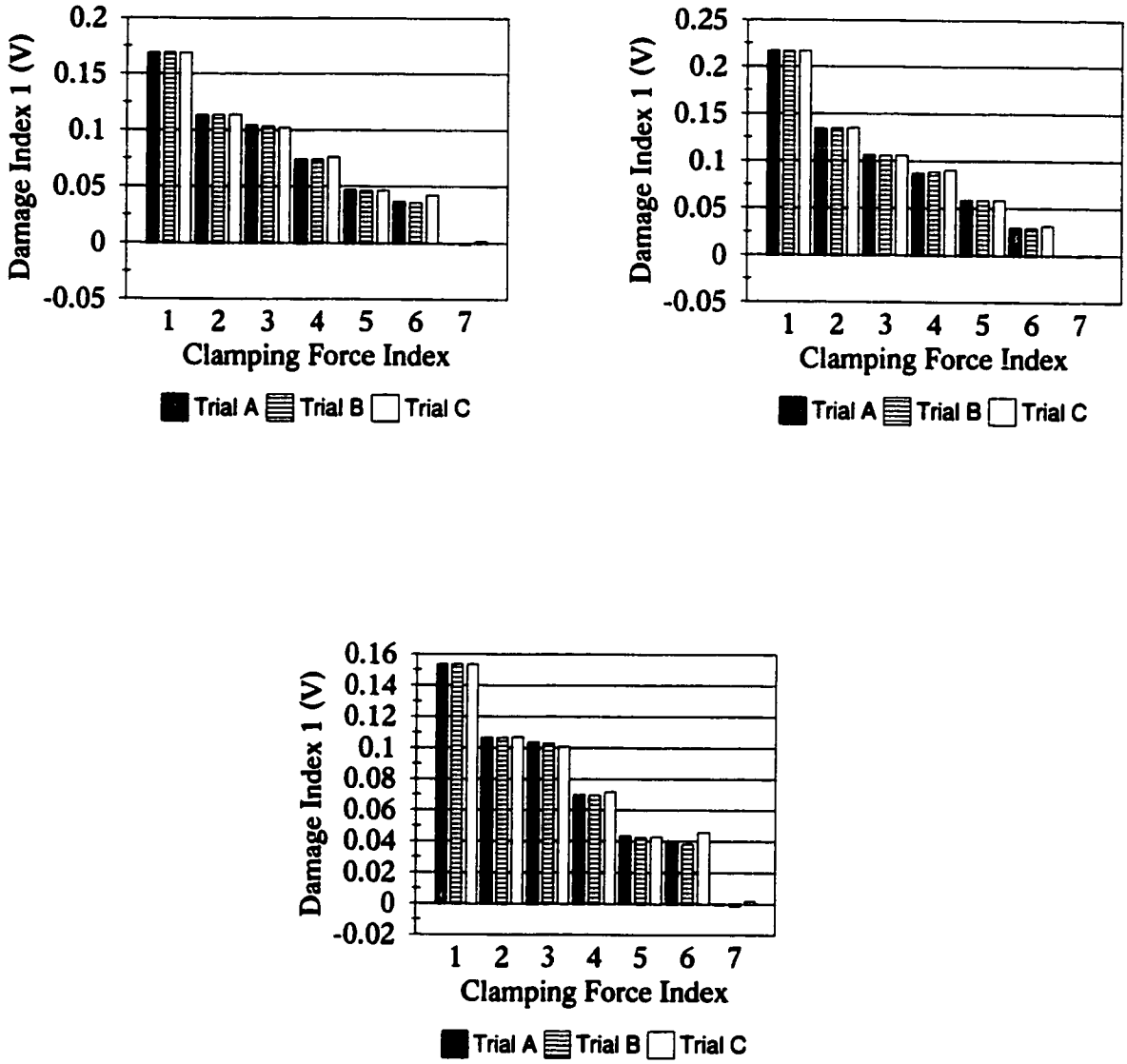

Figure 6.3: Type 1 damage index results based on all data samples - total response window (top left); excitation window (top right); and free vibration window (bottom).

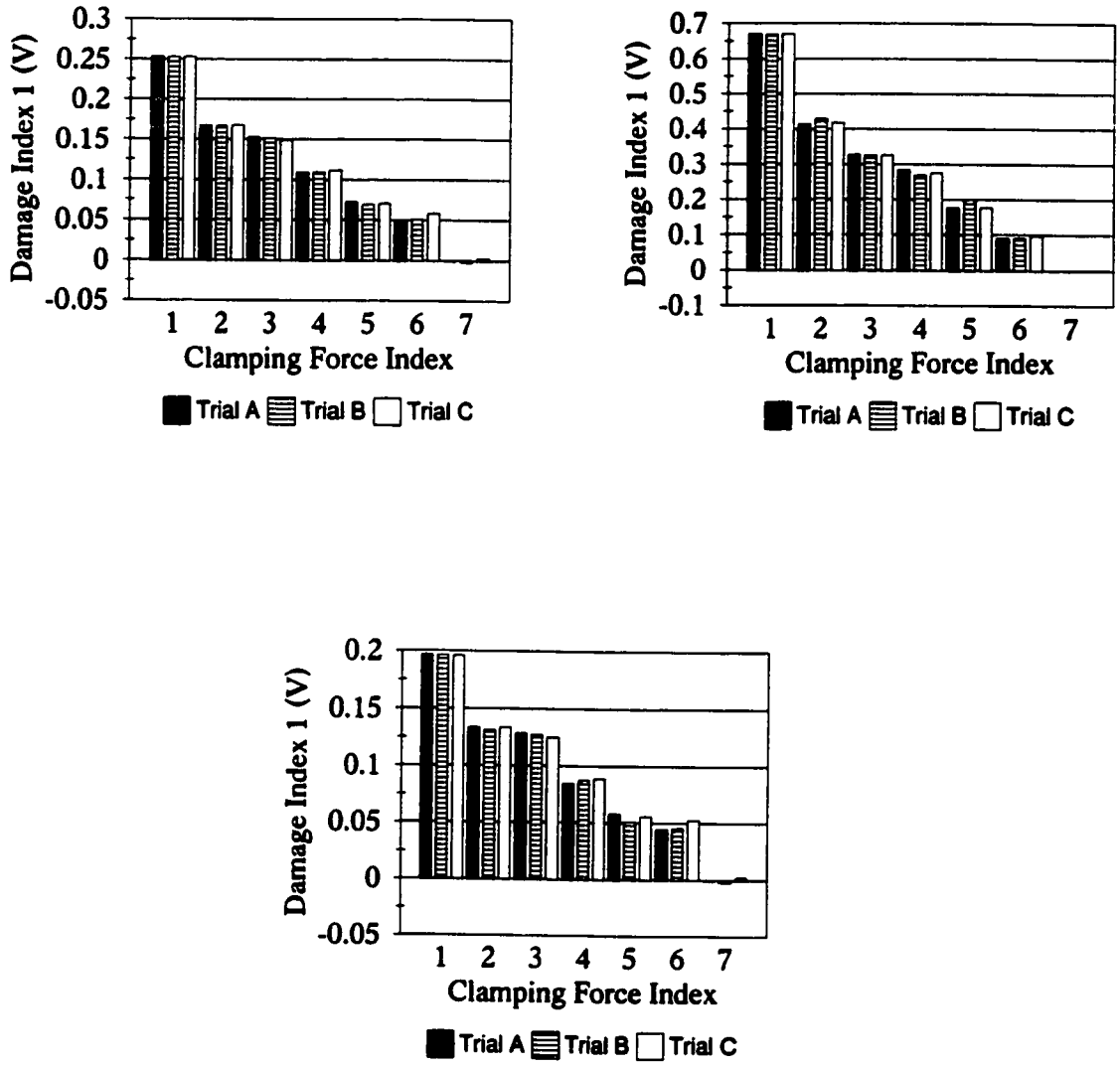

Figure 6.4: Type 1 damage index results based on only cycle maxima/minima - total response window (top left); excitation window (top right); and free vibration window (bottom).

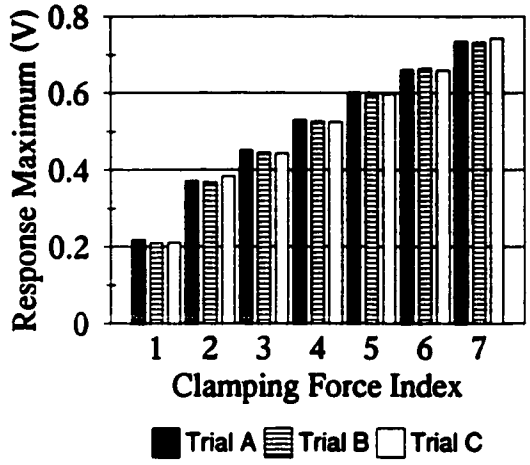

Figure 6.5: Type 2 (maximum amplitude) damage index results.

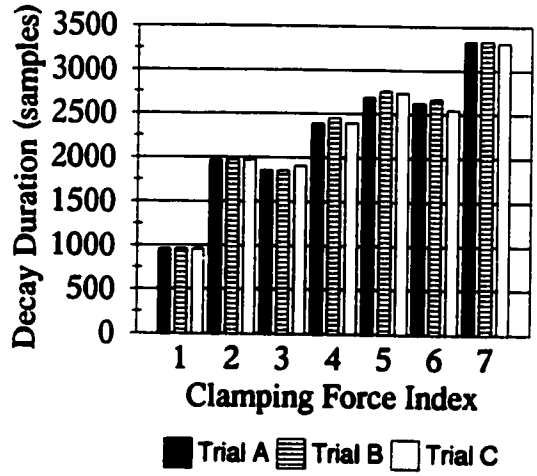

Figure 6.6: Type 3 (decay duration) damage index results.

6.4 Verification of Damage Index Criteria

In this section, the various damage index results are compared with respect to the criteria of Section 6.2.

6.4.1 Criterion 1 - Monotonical Correlation of Index with Clamping Force

Generally, all the Type 1 (overall response amplitude) damage index results satisfy this criterion. As the clamping force increases, the index value decreases indicating less damage in the connection. Only the results calculated using the free vibration time window have one or two index values which do not show a monotonical trend. Aside from this observation, without knowing the actual clamping force values it is difficult to judge whether using one time window or another is better, or whether using all data samples is better than using only cycle maxima/minima.

The Type 2 (maximum amplitude) index results also satisfy this first criterion. As the clamping force increases, the maximum amplitude of the response increases. However, the Type 3 (decay duration) index does not satisfy the criterion. It is found to have local decreases in its index value as the clamping force is increased, although the general trend of the curve is an increasing one.

6.4.2 Criterion 2 - Minimal Computation Requirements

Of the three general damage indices, the maximum amplitude and decay duration indices both

require minimal computation. The overall response amplitude damage index requires significant computation but this can be minimised by reducing the time window and the number of samples used for the calculation. Thus, in order to minimise computation the excitation zone should be used as the time window (instead of using the total response or free vibration zone), and only cycle maxima/minima should be used (instead of using all data samples).

6.4.3 Criterion 3 - Repeatability

In general, all the Type 1 damage indices have the same level of repeatability; this level is satisfactory in the sense that all three index values (Trial A, B and C) for any test case *i* are separated in value from the values of other test cases. Repeatability is found to degrade slightly if only cycle maxima/minima are used (instead of using all the data samples in the calculation of index). The best indices with respect to repeatability appear to be the overall response amplitude damage index for the excitation zone using all data samples, and the maximum amplitude damage index. The sample to decay index values are also satisfactorily repeatable.

6.4.4 Summary of Findings

The results of the damage analysis can be summarised in a few major points:

- Type 1 and 2 damage indices are monotonically related to the clamping force (i.e., loosening of connection).

- No significant differences exist in the results of the Type 1 index between using all data samples in calculation or only using the cycle maxima/minima.

6.4.5 Damage Index Selection

Final selection of a damage index depends on how the criteria (Sec. 6.2) are weighted. If it is assumed, for the present analysis, that all three criteria are of equal weight, the maximum amplitude damage index (Type 2) would be selected as the best index. The second best index is the overall response amplitude damage index (Type 1) based on cycle maxima/minima with the excitation zone time window.

6.5 Cutoff Voltage Level

As explained earlier in Section 6.3.1, the cutoff voltage level defines the end of the Calculation Time Windows 1 and 3. The repeatability of the results for these indices is significantly dependent on the value chosen for the cutoff voltage level. Thus, the repeatability can be improved by adjusting the cutoff level, which in turn affects the size and location of the time window for the index calculation. The value chosen for the present analysis corresponds to three times the maximum amplitude of the measurement noise. Factors of 1, 2, 2.5, 3.5 and 4 were all tried in analysis and none gave results as repeatable as those calculated using a cutoff level of three times the maximum noise amplitude.

The purpose of the cutoff level is twofold: (1) it prevents the measurement noise from

adversely affecting the higher damage cases (for which a significant portion of the response decay is below the maximum amplitude of the measurement noise); and (2) it provides a further means to improve the repeatability of the Type 1 index results.

Chapter 7

Conclusions and Recommendations

7.1 Conclusions

Several conclusions may be made regarding the research already presented:

1) Detectable differences are present in simulations and experiments between transient responses for the disconnected beam ($F_c = 0$), damaged beam ($0 < F_c < F_{secure}$) and the secure beam ($F_c = F_{secure}$). In experiment, differences are observed for the following transient response characteristics: overall response amplitude, maximum amplitude, and decay duration.

2) The differences in the responses of the various test cases can be quantified in terms of damage indices which can be used in practice to measure indirectly the level of damage to

structural connections. Based on the three criteria of Section 6.2 (monotonical relationship to clamping force; minimal computation requirements; repeatability), the maximum amplitude damage index was found to be the best index.

3) The results of experiments and simulations are found to agree in two important areas: natural frequencies and qualitative differences between disconnected and secure beam responses.

4) The proposed approach has definite advantages over current steady-state harmonic response based methods due to the fact that more information is available in the transient response of a structure. Since many of the characteristics of the transient response are not constant with respect to time, a multiple number of "time windows" can be used in designing a damage detection procedure. This should result in more effective and more reliable damage detection.

5) The proposed approach should be designed around an optimum excitation frequency corresponding to the secure case natural frequency furthest in value from the nearest two adjacent natural frequencies of the disconnected case for the structure.

7.2 Recommendations for Future Work

The following recommendations can be made to improve the effectiveness of the proposed approach in detecting damage in a real-life structure:

1) A single actuator/sensor device could be used per flexible component. As discussed in Section 2.3, piezo-elements have the capabilities of actuating and sensing mechanical deformation. Therefore, one element may be used for exciting and subsequently sensing the flexural vibrations of the component tested. This would reduce equipment costs substantially for structures containing a large number of components. One possible disadvantage of using one element for actuating/sensing is that the excitation zone time window of the transient response can no longer be used for damage analysis.

2) For implementation, more than one index might be have used in the damage detection process to ensure accurate results.

3) Several time windows should be investigated in the design of the damage analysis scheme to optimize its effectiveness. Only three obvious windows were explored in the present research.

4) With respect to the present research, damage to the variable beam connection should be quantified in terms of bolt torque so that a more accurate determination of the relationship between the various damage indices and the clamping force can be made. This would require sufficient amplification of the voltage signal to the actuator since for constant clamping force as the excitation amplitude is increased so does the apparent looseness of the connection. This would ensure that the clamping forces of all damaged cases (i=2 to 6) correspond to bolt torques which are large enough to be measured by a standard torque wrench.

References

Adams, R.D., P. Cawley, C.J. Pye, and B.J. Stone. 1978. A vibration technique for non-destructively assessing the integrity of structures. *Journal Mechanical Engineering Science* 20, no. 2:93-100.

Brock, J.E. 1968. Optimal matrices describing linear systems. *AIAA Journal* 6, no. 7:1292-1296.

Cattarius, J., and D.J. Inman. 1997. Time domain analysis for damage detection in smart structures. *Mechanical Systems and Signal Processing* 11, no. 3: 409-423.

Cawley, P., and R.D. Adams. 1979. The location of defects in structures from measurements of natural frequencies. *Journal of Strain Analysis* 14, no. 2:49-57.

Crawley, E.F. 1994. Intelligent structures for aerospace: A technology overview and assessment. *AIAA Journal* 32, no. 8:1689-1699.

de Benedetti, M., and R. Barboni. 1998. On the modelisation of the piezoelectric effect with control system and some applications. In *Proceedings of the first international conference on computational methods for smart structures and materials*, ed. P. Santini, M. Marchetti, and C.A. Brebbia, 3-23. Rome, Italy: WITPress Computational Mechanics Publications.

Doebelin, E.O. 1990. *Measurement systems - application and design*. 4th ed. McGraw-Hill.

Doebling, S.W. 1996. Minimum-rank optimal update of elemental stiffness parameters for structural damage identification. *AIAA Journal* 34, no. 12:2615-2621.

dSPACE digital signal processing and control engineering GmbH. 1990. *DSP-CITpro hardware and TRACE Manuals*. Paderborn, Germany.

Fritzen, C.-P., D. Jennewein, and Th. Kiefer. 1997. Damage detection based on vibration measurements and inaccurate models. In *Proceedings of the 1997 ASME design engineering technical conferences*, 1-12. Sacramento, California: ASME.

Gandhi, M.V., and B.S. Thomson. 1992. *Smart materials and structures*. London: Chapman and Hall.

Giurgiutiu, V., and C.A. Rogers. 1997. Electro-mechanical (E/M) impedance method for structural health monitoring and non-destructive evaluation. In *Proceedings of the international workshop on structural health monitoring*. ed. F.-K. Chang, 433-444. Stanford, California: Technomic.

Goldfarb, M., and N. Celanovic. 1996. Modeling piezoelectric stack actuators for control of micromanipulation. In *Proceedings of the 1996 IEEE international conference on robotics and automation*, 69-79. Minneapolis, Montana.

Gorman, D.J. 1975. *Free vibration analysis of beams and shafts*. New York: John Wiley & Sons.

Graff, K.F. 1975. *Wave motion in elastic solids*. London: Oxford University Press.

Hagood, N.W., and A. von Flotow. 1991. Damping of structural vibrations with piezoelectric materials and passive electrical networks. *Journal of Sound and Vibration* 146, no. 2:243-268.

Hagood, N.W., W.H. Chung, and A. von Flotow. 1990. Modelling of piezoelectric actuator dynamics for active structural control. *Journal of Intelligent Material System and Structures* 1: 327-354.

Housner, G.W., L.A. Bergman, T.K. Caughey, A.G. Chassiakos, R.O. Claus, S.F. Masri, R.E. Skelton, T.T. Soong, B.F. Spencer, and J.T.P Yao. 1997. Structural control: past, present, and future. *Journal of Engineering Mechanics* 123, no. 9.

Inman, D. 1994. *Engineering vibration*. Englewood Cliffs, New Jersey: Prentice Hall.

Iong, K.-V. 1997. Smart Structure Integrity Monitoring using Transient Response. M.A.Sc. Thesis, University of Ottawa.

Islam, A.S., and K.C. Craig. 1994. Damage detection in composite structures using piezoelectric materials. *Smart Mater. Struct.* 3:318-328.

Jian, X.H., H.S. Tzou, C.J. Lissenden, and L.S. Penn. 1997. Damage detection by piezoelectric patches in a free vibration method. *Journal of Composite Materials* 31, no. 4:345-359.

Juneja, V., R.T. Haftka, and H.H. Cudney. 1997. Damage detection and damage detectability - analysis and experiments. *Journal of Aerospace Engineering* 10, no. 4:135-142.

Kabe, A.M. 1985. Stiffness matrix adjustment using mode data. *AIAA Journal* 23, no. 9:1431-1436.

Kaouk, M., and D.C. Zimmerman. 1994. Structural damage assessment using a generalized minimum rank perturbation theory. *AIAA Journal* 32, no. 4:836-842.

Lancaster, D. 1996. *Active filter cookbook*. 2nd ed. Oxford: Newnes.

Liang, C., F.P. Sun, and C.A. Rogers. 1994a. An impedance method for dynamic analysis of active material systems. *Transactions of the ASME - Journal of Vibration and Acoustics* 116: 120-128.

----------. 1994b. Electro-mechanical impedance modeling of active material systems. *SPIE* 2192: 232-253.

Lim, T.W. 1995. Structural damage detection using constrained eigenstructure assignment. *Journal of Guidance, Control, and Dynamics* 18, no. 3:411-418.

Lim, T.W., and T.A.L. Kashangaki. 1994. Structural damage detection of space truss structures using best achievable eigenvectors. *AIAA Journal* 32, no. 5:1049-1057.

Lim, T.W., A. Bosse, and S. Fisher. 1996. Structural damage detection using real-time modal parameter identification algorithm. *AIAA Journal* 34, no. 11:2370-2376.

Manning, R.A. 1994. Structural damage detection using active members and neural networks. *AIAA Journal* 32, no. 6:1331-1333.

Necsulescu, D. 1996. *Health monitoring of space structures using high frequency mechanical impedance estimation*. Final Report, C.S.A. Contract.

Necsulescu, D., and R. DeAbreu. 1998. *Multi-sensor integrity monitoring of space structures using wave propagation and steady-state harmonic response approaches.* Report, C.S.A. Contract.

Necsulescu, D.S., R.F. De Abreu, and F. Bakhtiari-Nejad. 1998. Smart structure monitoring using transient response. In *Proceedings of the first international conference on computational methods for smart structures and materials*, ed. P. Santini, M. Marchetti, and C.A. Brebbia, 141-150. Rome, Italy: WITPress Computational Mechanics Publications.

Pandey, A.K., and M. Biswas. 1994. Damage detection in structures using changes in flexibility. *Journal of Sound and Vibration* 169, no. 1:3-17.

Pandey, A.K., M. Biswas, and M.M. Samman. 1991. Damage detection from changes in curvature mode shapes, *Journal of Sound and Vibration* 145, no. 2:321-332.

Prasad, S.E. 1995. *Piezoelectric ceramics - product catalogue and application notes*. Collingwood, Ontario: Sensor Technology Limited.

Rizos, P.F., N. Aspragathos, and A.D. Dimarogonas. 1990. Identication of crack location and magnitude in a cantilever beam from the vibration modes. *Journal of Sound and Vibration* 138, no. 3:381-388.

Rogers, C.A. 1990. An introduction to intelligent material systems and structures. *Intelligent Structures*. Elsevier Applied Science Publishers Ltd., 3-37.

Standards committee of the IEEE Ultrasonics, Ferroelectrics, and Frequency Control Society. 1987. *An american national standard: IEEE standard on piezoelectricity*. New York: The Institute of Electrical and Electronics Engineers, ANSI/IEEE Std. 176-1987.

Sun, F.P., C. Liang, and C.A. Rogers. 1994. Structural modal analysis using collocated actuator/sensors - an electromechanical approach. *SPIE* 2190:238-249.

Sun, F.P., Z. Chaudry, C. Liang, and C.A. Rogers. 1995. Truss structure integrity identification using PZT sensor-actuator. *Journal of Intelligent Material Systems and Structures* 6:134-139.

Timoshenko, S., D.H. Young, and W. Weaver. 1974. *Vibration problems in engineering*. 4th ed. New York: John Wiley & Sons.

Tsou, P., and M.-H. Herman Shen. 1994. Structural damage detection and identification using neural networks. *AIAA Journal* 32, no. 1:176-183.

Appendix A

Transient Responses of the Beam from Experiment

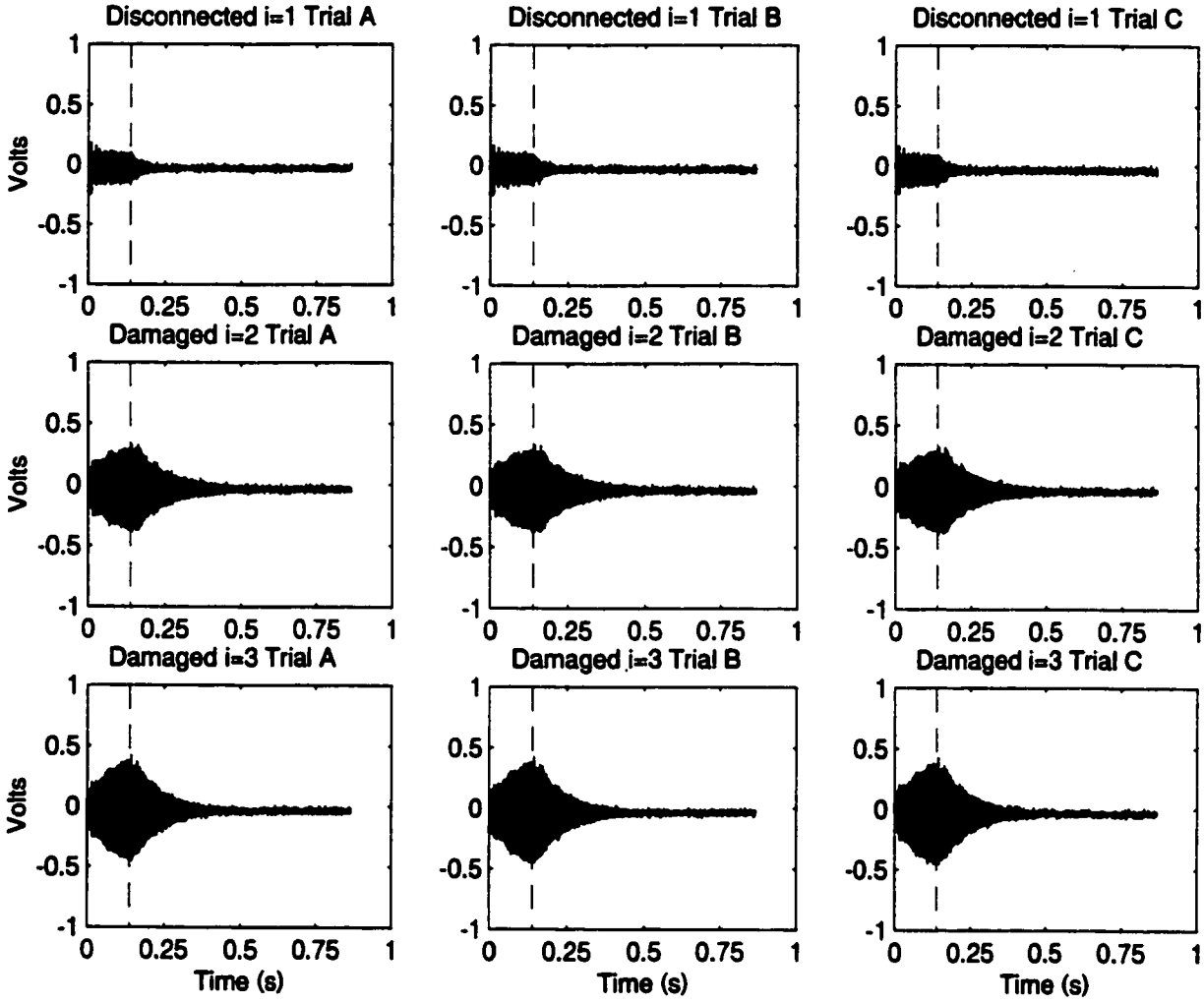

Figure A.1: Unfiltered transient responses of the beam for test cases $i = 1$ to 3.

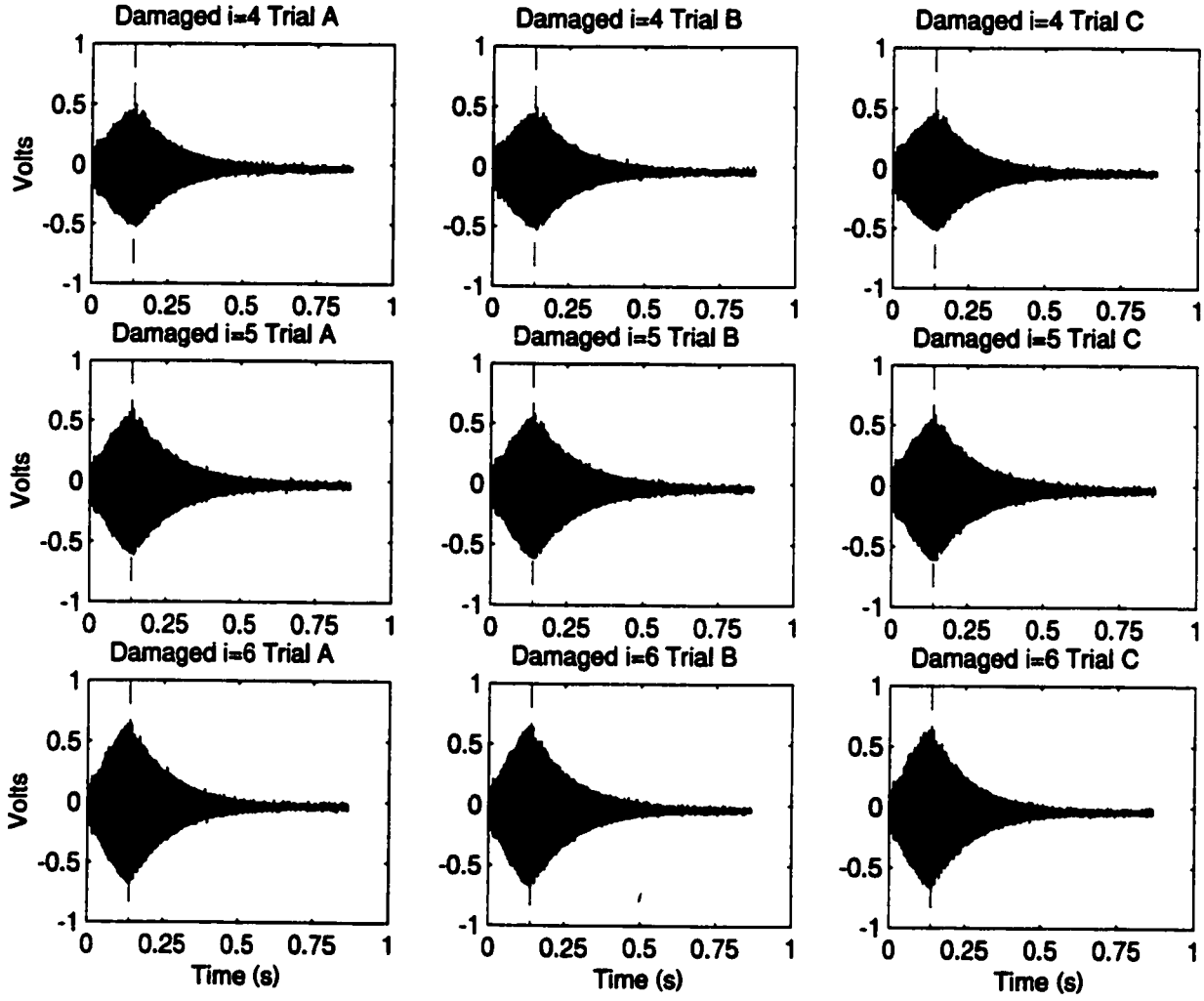

Figure A.2: Unfiltered transient responses of the beam for test cases $i = 4$ to 6.

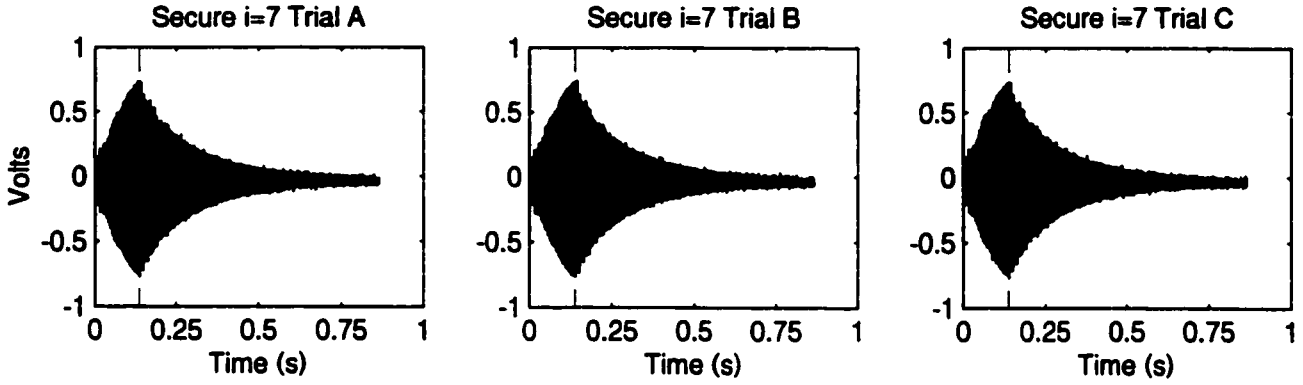

Figure A.3: Unfiltered transient responses of the beam for test case $i = 7$ (secure).

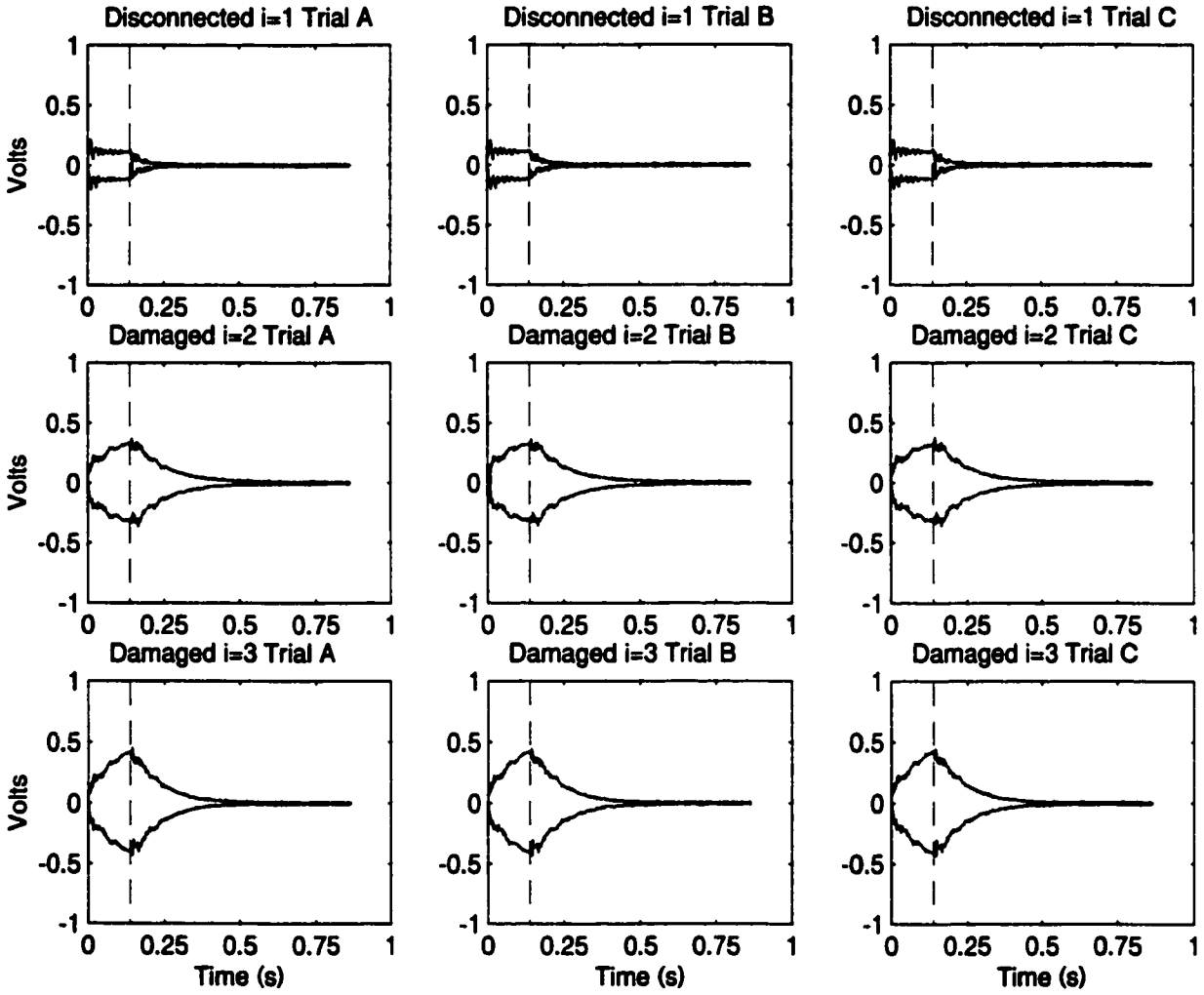

Figure A.4: Filtered transient responses (cycle maxima/minima only) of the beam for test cases $i = 1$ to 3.

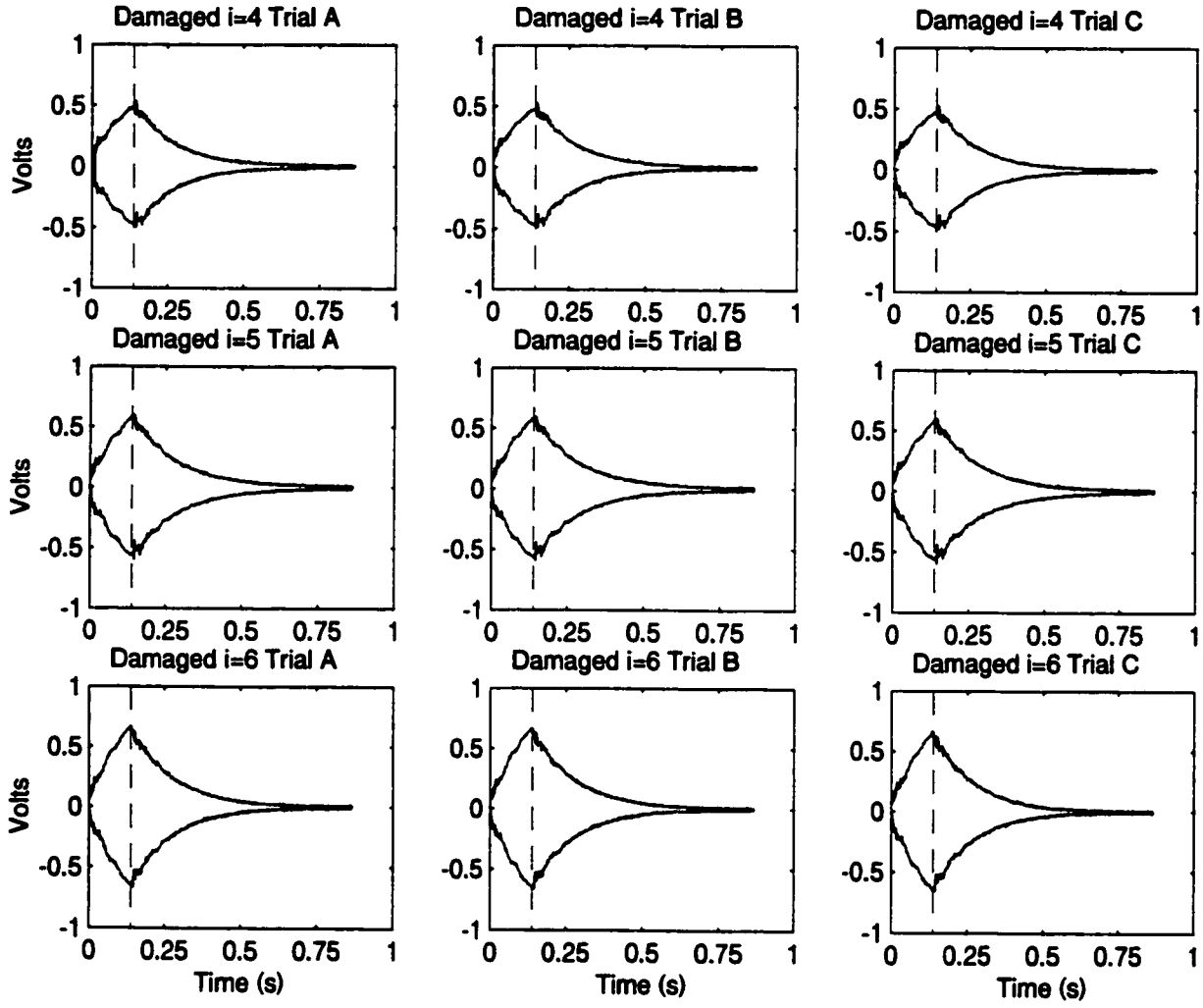

Figure A.5: Filtered transient responses (cycle maxima/minima only) of the beam for test cases $i = 4$ to 6.

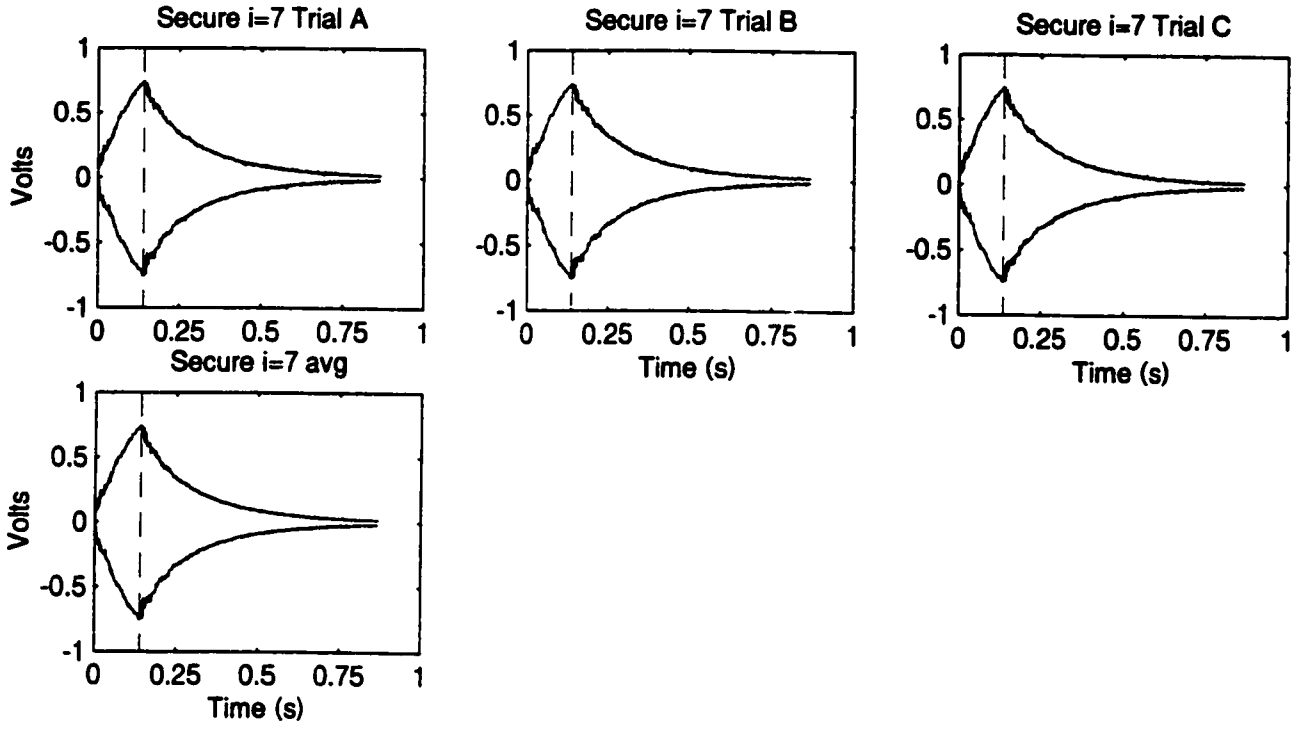

Figure A.6: Filtered transient responses (cycle maxima/minima only) of the beam for test case $i = 7$ (secure) and sample-by-sample average secure case response.

Appendix B

Damage Index Results

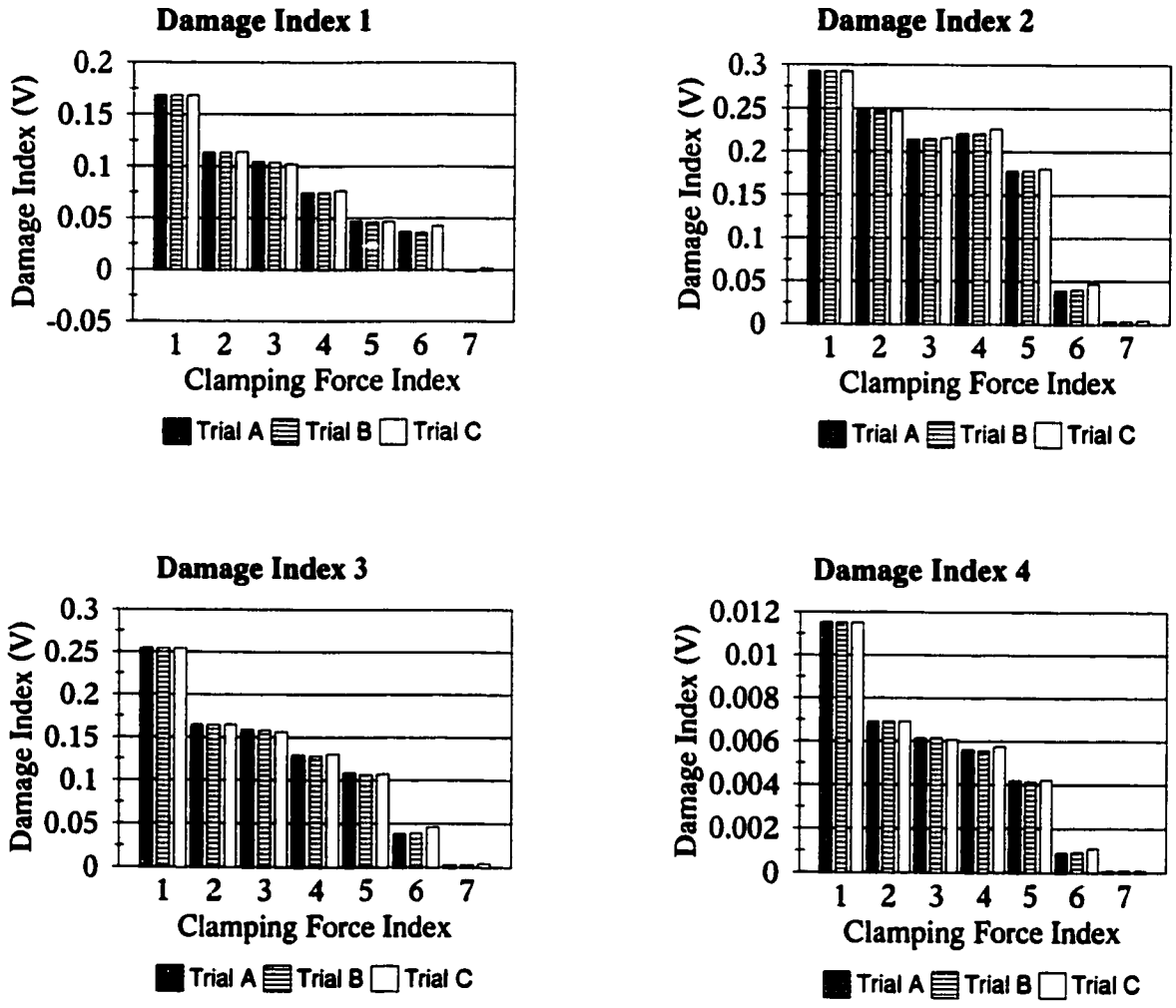

Figure B.1: Results for Type 1 damage indices calculated based on all data samples and using Time Window 1 (total response).

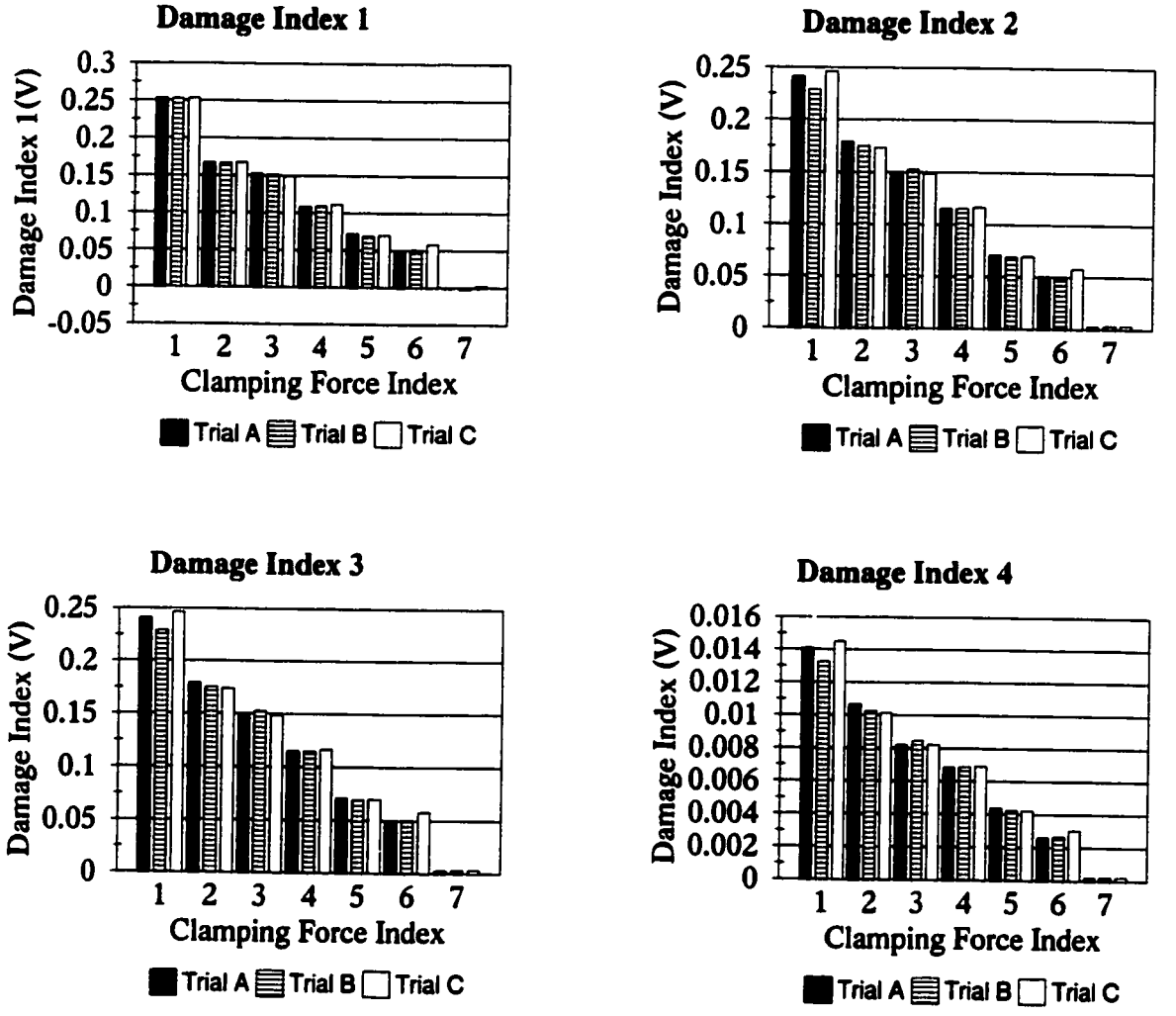

Figure B.2: Results for Type 1 damage indices calculated based on cycle maxima/minima and using Time Window 1 (total response).

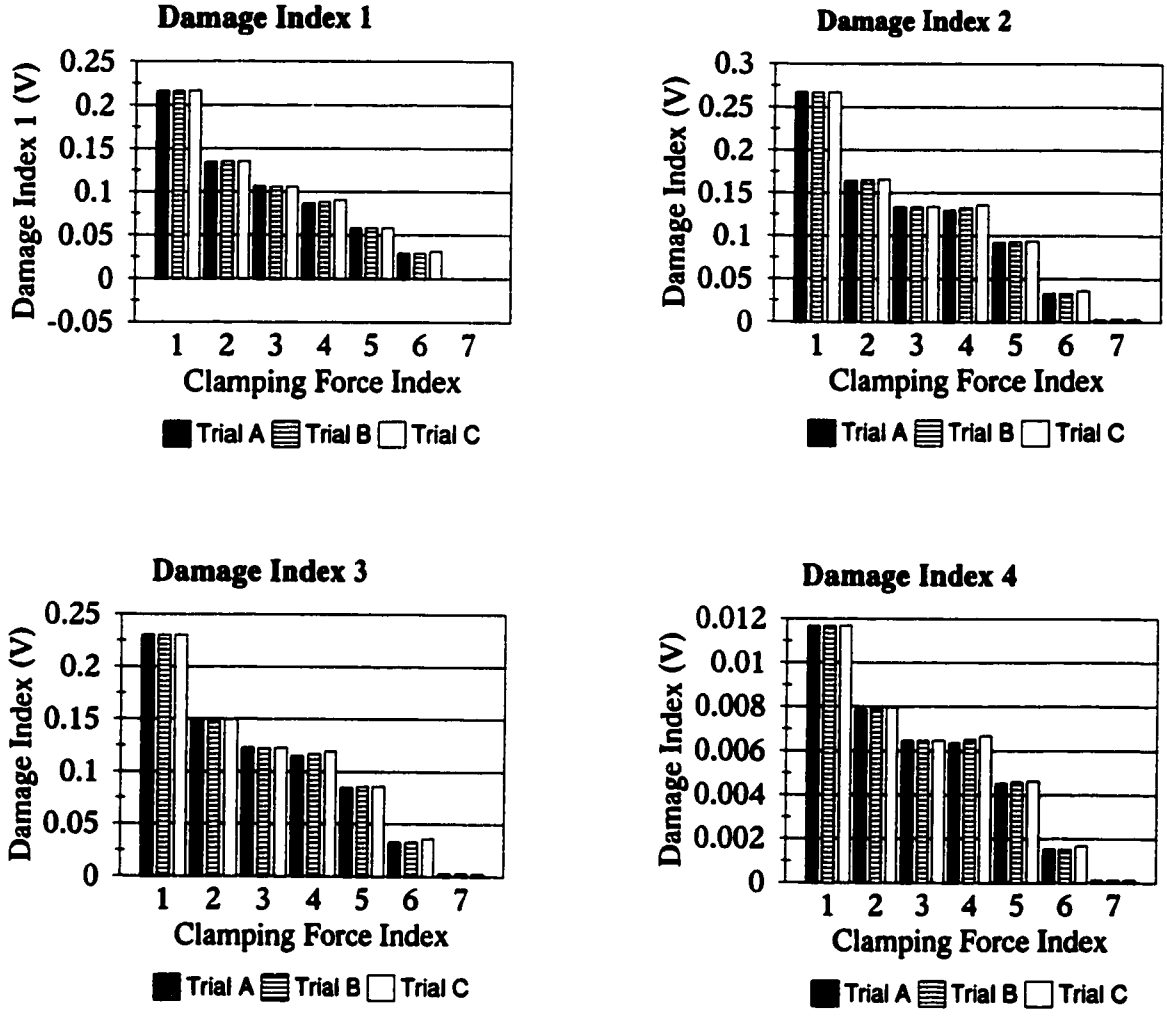

Figure B.3: Results for Type 1 damage indices calculated based on all data samples and using Time Window 2 (excitation zone).

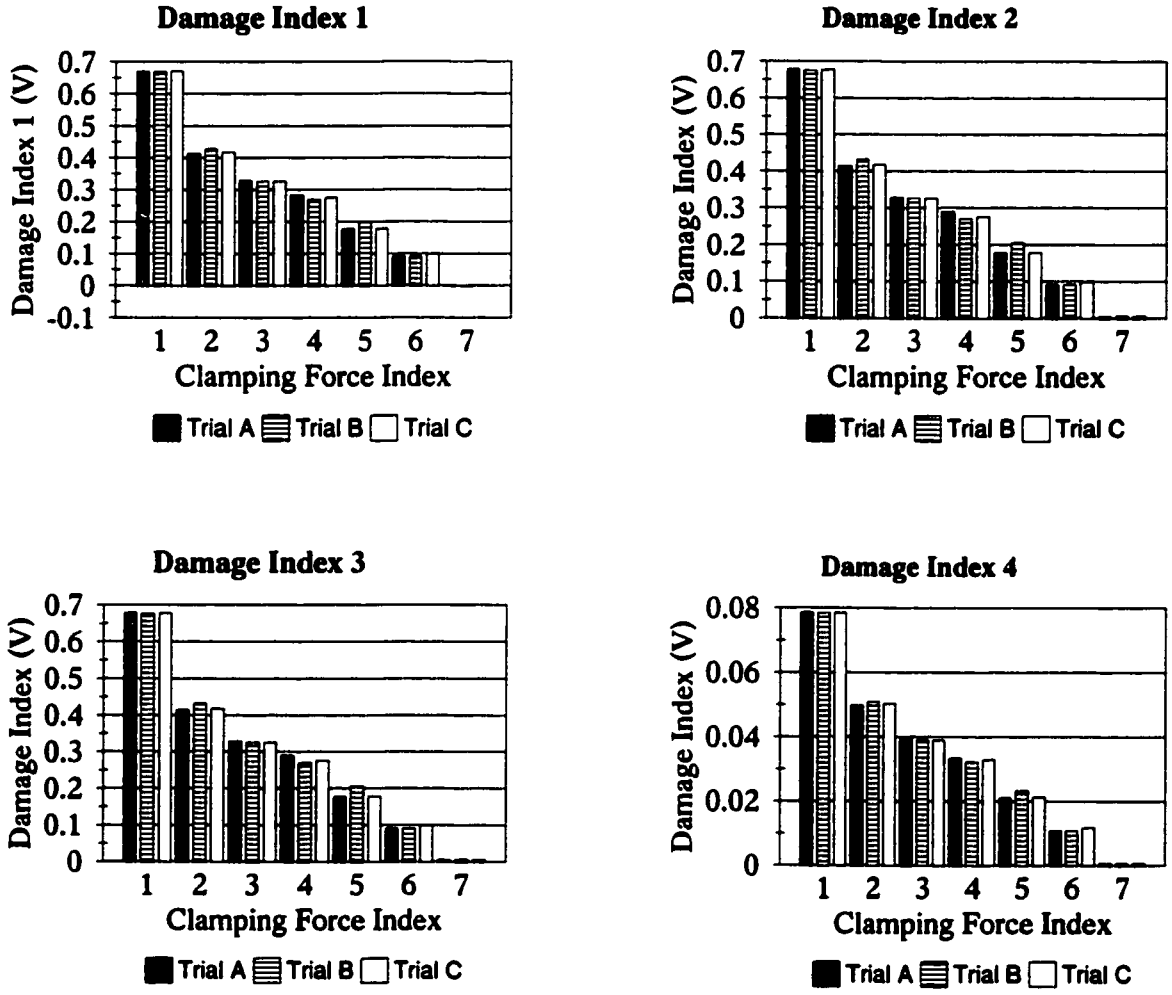

Figure B.4: Results for Type 1 damage indices calculated based on cycle maxima/minima and using Time Window 2 (excitation zone).

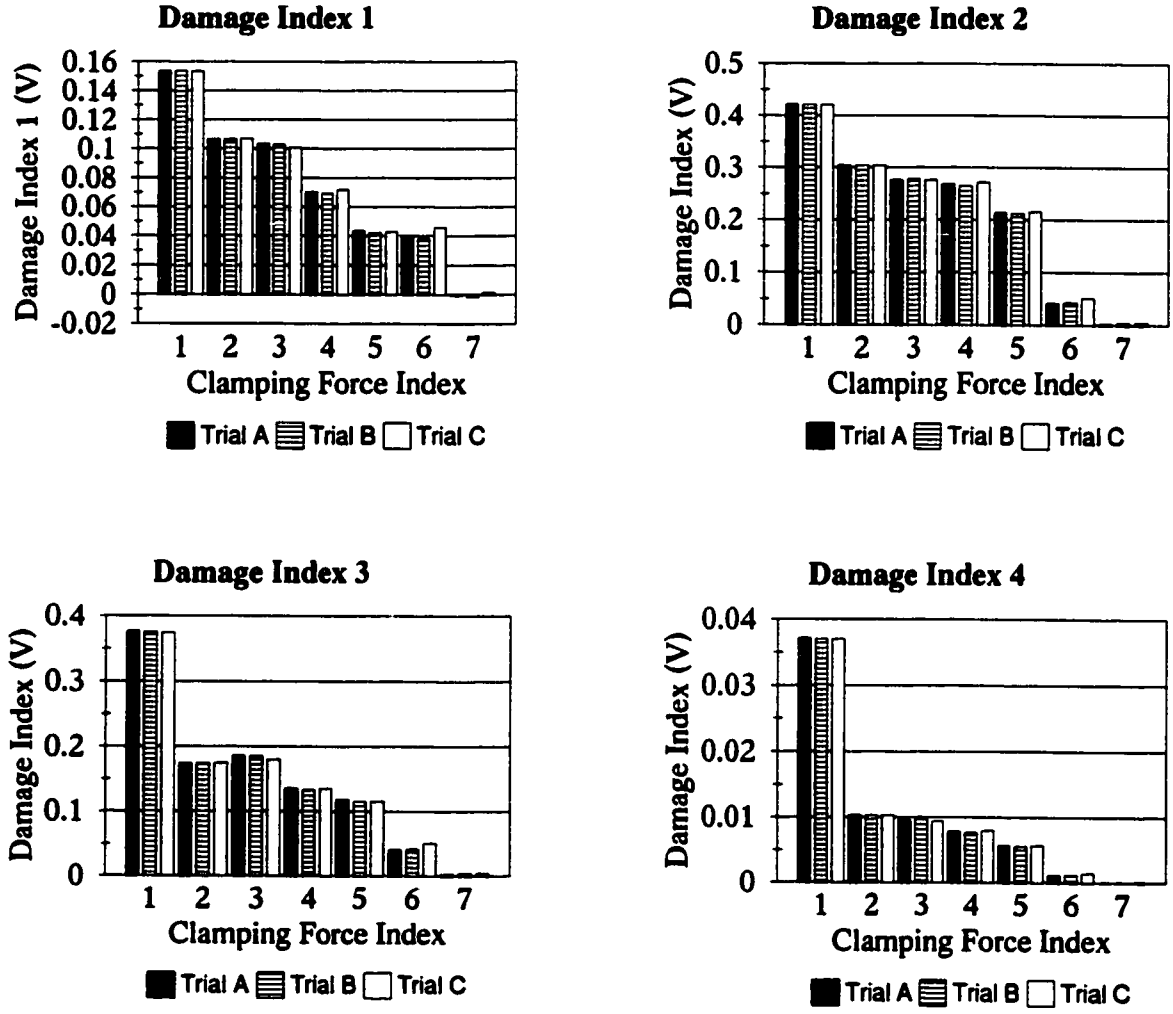

Figure B.5: Results for Type 1 damage indices calculated based on all data samples and using Time Window 3 (free vibration zone).

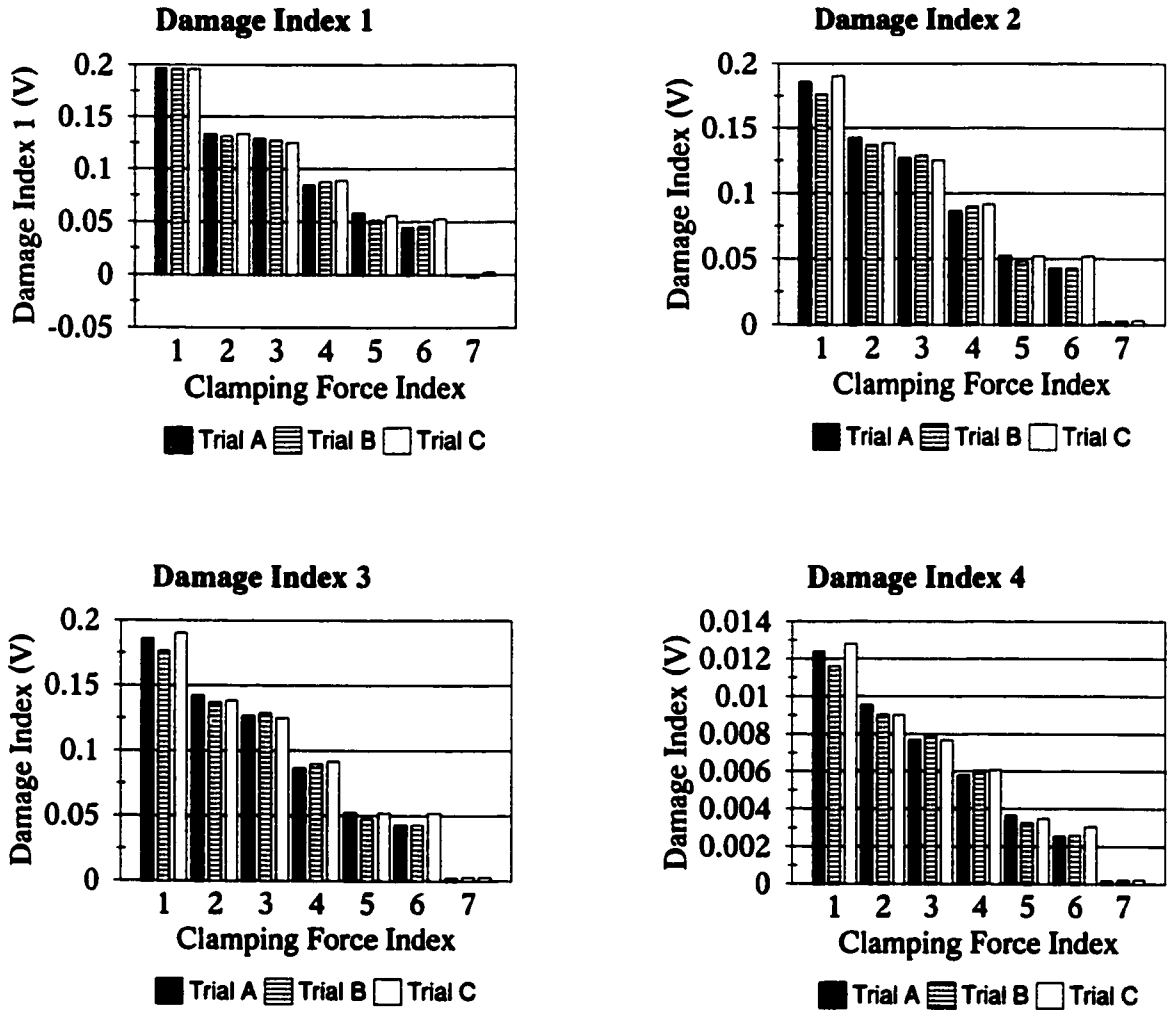

Figure B.6: Results for Type 1 damage indices calculated based on cycle maxima/minima and using Time Window 3 (free vibration zone).

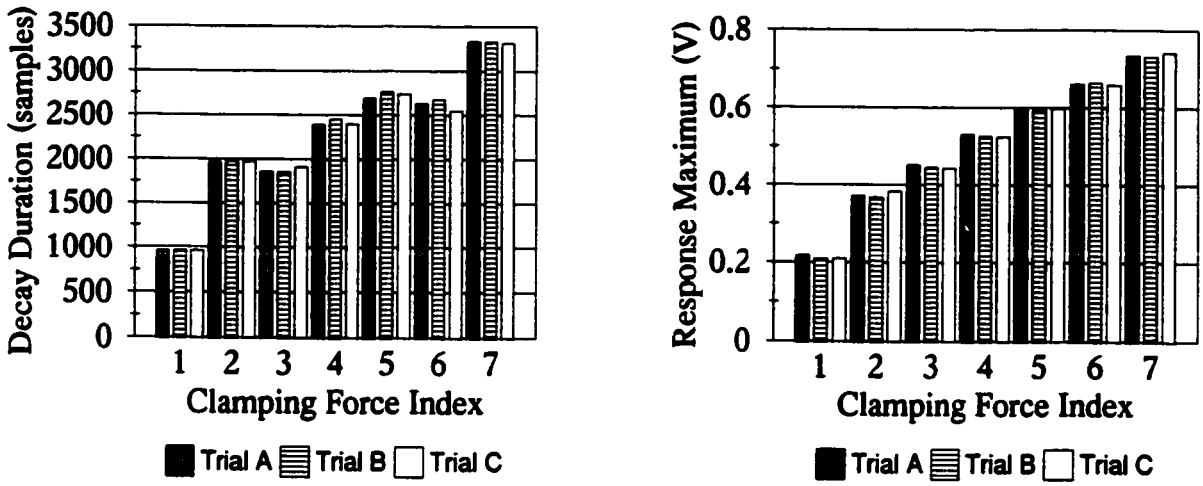

Figure B.7: Results for Type 2 (maximum response amplitude) and Type 3 (decay duration) damage indices.

Appendix C

MATLAB M-File Programs

C.1 Simulation Program

```
%%%%%%%%%%%%%%%%%%%%%%%%%%%%%%%%%%%%%%%%%%%%%%%%%%%%%%%%%%%%%%%%%%%%%%%%%%%%
%
%       MATLAB m-file program
%               - to determine natural frequencies of the beam (Section 4.2)
%               - to simulate the transient response of a thin beam to a sinusoidal transverse excitation of a
%                 finite number of cycles for a fixed-fixed and cantilever boundary condition case (Section 4.4).
%
%       NOTE: Cut off series calculation with .01% convergence criterion ONLY AFTER 'natfr(i)'>'omega'
%               (since there is a large increase in 'yt()' when natfr(i) approaches 'omega')
%
%       NOTE: Nearest fixed-fixed 'natfr' to 'excfr' is 373.28 Hz. Nearest cantilever 'natfr' to 'excfr' is 416.7 Hz.
%
%%%%%%%%%%%%%%%%%%%%%%%%%%%%%%%%%%%%%%%%%%%%%%%%%%%%%%%%%%%%%%%%%%%%%%%%%%%%

clear;

%%%%%%%%%%%%%%%%%%%%%%%%%%%%%%%%%%%%%%%%%%%%%%%%%%%%%%%%%%%%%%%%%%%%%%%%%%%%
%
%       INPUT constants
%                                                        fixed-fixed      cantilever
%
%       len = clamped length of beam [m]            =      0.496            0.5465
%       fileadd                                     =      'cc374'          'cf374'
%       xsen = distance to sensor [m]
%       xact = distance to actuator [m]
%       cycles = number of excitation cycles
%       alpha = transverse excitation acceleration [m/s^2]
```

```
%       ym = elastic modulus of aluminum [N/m^2]
%       rmoi = rectangular moment of inertia of cross-section [m^4]
%       rho = density of aluminum [kg/m^3]
%       area = cross-sectional area of beam [m^2]
%
%%%%%%%%%%%%%%%%%%%%%%%%%%%%%%%%%%%%%%%%%%%%%%%%%%%%%%%%%%%%%%%%

excfr=374.5;
responsetime=0.8;
samples_per_excycle=16;
len=.5465;
fileadd='cf374';
xsen=.1889;
xact=.1270;
cycles=50;
alpha=1;
ym=71.5e9;
rmoi=1.753e-12;
rho=2750;
area=23.8e-6;
cutoff=.0001;


%%%%%%%%%%%%%%%%%%%%%%%%%%%%%%%%%%%%%%%%%%%%%%%%%%%%%%%%%%%%%%%%
%
%       CALCULATE constants:        a [m^2/s]
%                                   omega = excitation frequency [radians]
%                                   texc = time duration of excitation [s]
%                                   fs = sampling frequency [Hz]
%                                   samples = total number of samples for beam response
%
%%%%%%%%%%%%%%%%%%%%%%%%%%%%%%%%%%%%%%%%%%%%%%%%%%%%%%%%%%%%%%%%

a=sqrt(ym*rmoi/(rho*area));
omega=2*pi*excfr;
texc=cycles/excfr;
fs=samples_per_excycle*excfr;
samples=fs*responsetime;


%%%%%%%%%%%%%%%%%%%%%%%%%%%%%%%%%%%%%%%%%%%%%%%%%%%%%%%%%%%%%%%%
%
%       CALCULATE frequency parameters (beta_l = beta*len)
%
%%%%%%%%%%%%%%%%%%%%%%%%%%%%%%%%%%%%%%%%%%%%%%%%%%%%%%%%%%%%%%%%

if (fileadd(2)=='c'),
  beta_l(1)=4.7300;
  beta_l(2)=7.8532;
  beta_l(3)=10.9956;
else
  beta_l(1)=1.8751;
```

```
   beta_l(2)=4.6941;
   beta_l(3)=7.8548;
 end
 for n=3:300,
   beta_l(n)=beta_l(n-1)+pi;
 end
 n=1


%%%%%%%%%%%%%%%%%%%%%%%%%%%%%%%%%%%%%%%%%%%%%%%%%%%%%%%%%%%%%%%%%%%%%%
%
%       TIME INCREMENT LOOP           tt = 1-D time array
%                                     t = time value
%                                     i,j = counters
%
%%%%%%%%%%%%%%%%%%%%%%%%%%%%%%%%%%%%%%%%%%%%%%%%%%%%%%%%%%%%%%%%%%%%%%

for i=1:samples,
  i
  tt(i)=i*(1/fs);
  t=tt(i);


%%%%%%%%%%%%%%%%%%%%%%%%%%%%%%%%%%%%%%%%%%%%%%%%%%%%%%%%%%%%%%%%%%%%%%
%
%       INITIALIZE array values
%
%%%%%%%%%%%%%%%%%%%%%%%%%%%%%%%%%%%%%%%%%%%%%%%%%%%%%%%%%%%%%%%%%%%%%%

  for k=1:n,
    Tfunc(k)=0.;
    yt(k)=0.;
  end

%%%%%%%%%%%%%%%%%%%%%%%%%%%%%%%%%%%%%%%%%%%%%%%%%%%%%%%%%%%%%%%%%%%%%%
%
%       CALCULATE initial term of response series expression (n=1):
%
%               natfr = array of natural frequencies
%               b = nth beta value
%               X_act = array of beam mode shape values at actuator location
%               X_sen = array of beam mode shape values at sensor location
%               Tfunc = array of values of the time-dependent function in the response expression
%               yt = array of the response series expression values
%
%%%%%%%%%%%%%%%%%%%%%%%%%%%%%%%%%%%%%%%%%%%%%%%%%%%%%%%%%%%%%%%%%%%%%%

  n=1;
  bl=beta_l(n);
  b=bl/len;
  natfr(n)=a*b^2;
  bs=b*xsen;
```

```
    ba=b*xact;
    if (fileadd(2)=='c'),
       X_const=(cosh(bl)-cos(bl))/(sinh(bl)-sin(bl));
    else
       X_const=(sinh(bl)-sin(bl))/(cosh(bl)+cos(bl));
    end
    X_act(n)=X_const*(sinh(ba)-sin(ba))-cosh(ba)+cos(ba);
    X_sen(n)=X_const*(sinh(bs)-sin(bs))-cosh(bs)+cos(bs);
    Tfunc(n)=natfr(n)*(sin(omega*texc)*cos(natfr(n)*(t-texc)))+omega*(cos(omega*texc)*sin(natfr(n)*(t-texc))
                   -sin(natfr(n)*t));
    yt(n)=(2*alpha/len)*X_act(n)*X_sen(n)*Tfunc(n)/(natfr(n)*(natfr(n)^2-omega^2));


%%%%%%%%%%%%%%%%%%%%%%%%%%%%%%%%%%%%%%%%%%%%%%%%%%%%%%%%%%%%%%
%
%        "CALCULATION OF RESPONSE SERIES SUMMATION" LOOP
%
%%%%%%%%%%%%%%%%%%%%%%%%%%%%%%%%%%%%%%%%%%%%%%%%%%%%%%%%%%%%%%

   endloop=0;
   while (endloop==0),
      n=n+1;
      bl=beta_l(n);
      b=bl/len;
      natfr(n)=a*b^2;
      bs=b*xsen;
      ba=b*xact;
      if (fileadd(2)=='c'),
         X_const=(cosh(bl)-cos(bl))/(sinh(bl)-sin(bl));
      else
         X_const=(sinh(bl)-sin(bl))/(cosh(bl)+cos(bl));
      end
      X_act(n)=X_const*(sinh(ba)-sin(ba))-cosh(ba)+cos(ba);
      X_sen(n)=X_const*(sinh(bs)-sin(bs))-cosh(bs)+cos(bs);
      Tfunc(n)=natfr(n)*(sin(omega*texc)*cos(natfr(n)*(t-texc)))+omega*(cos(omega*texc)*
                  sin(natfr(n)*(t-texc))-sin(natfr(n)*t));
      yt(n)=yt(n-1)+(2*alpha/len)*X_act(n)*X_sen(n)*Tfunc(n)/(natfr(n)*(natfr(n)^2-omega^2));
      if ((abs((yt(n)-yt(n-1))/yt(n))<cutoff)&(natfr(n-1)>omega)),
         endloop=1;
      end
   end

% y = array of beam response values wrt time

   y(i)=yt(n);

end
y
plot(tt,y)
ylabel('Tranverse Displacement of Beam at Sensor (m)')
xlabel('Time (s)')
```

```
%%%%%%%%%%%%%%%%%%%%%%%%%%%%%%%%%%%%%%%%%%%%%%%%%%%%%%%%%%%%%%%%%%%%%%%%
%
%       WRITE data to files
%
%%%%%%%%%%%%%%%%%%%%%%%%%%%%%%%%%%%%%%%%%%%%%%%%%%%%%%%%%%%%%%%%%%%%%%%%

z='%15.12f ';
d1='c:\arob\finalp~1\output\simu\';
n1='\n';
frmt=[z z n1];
respdata=[tt
y];
fid=fopen([d1 fileadd 'sim.out'],'w');
count=fprintf(fid,frmt,respdata)
fclose(fid)
fid=fopen([d1 fileadd 'nfr.out'],'w');
count=fprintf(fid,[z n1],natfr/(2*pi))
fclose(fid)
```

C.2 Damage Analysis Program

```
%%%%%%%%%%%%%%%%%%%%%%%%%%%%%%%%%%%%%%%%%%%%%%%%%%%%%%%%%%%%
%
%       MATLAB m-file program to
%               - calculate damage indices (Type 1, 2 and 3)
%               - plot transient responses measured in experiment
%               - plot damage indices
%               - write results to ascii file for plotting and checking in Quattro Pro
%
%%%%%%%%%%%%%%%%%%%%%%%%%%%%%%%%%%%%%%%%%%%%%%%%%%%%%%%%%%%%

clear;

%%%%%%%%%%%%%%%%%%%%%%%%%%%%%%%%%%%%%%%%%%%%%%%%%%%%%%%%%%%%
%
%       INPUT experimental parameters and data
%
%%%%%%%%%%%%%%%%%%%%%%%%%%%%%%%%%%%%%%%%%%%%%%%%%%%%%%%%%%%%

fname='data50.dat';
respno=21;
excycles=50;
colfactor=3;
outputflag='y';
noisyflag='y';
%
excfr=361;
fs=5776;
secure=respno+1;
samples=5001;
filterno=2;
noiseno=2;
firstsample=1;
firstmaxmin=1;
endsample_of_excn=excycles*fs/excfr;
endcycle_of_excn=excycles;
d2='c:\arob\finalp~1\';
%
fid=fopen([d2 fname],'r');
alldata = fread(fid,[samples,respno],'float');
fclose(fid)
fid=fopen([d2 'rnoise.dat'],'r');
noisedata = fread(fid,[samples,noiseno],'float');
fclose(fid)
%
% Reverse order of Data so that "disc." is first and "secure" is last
%
temp2=alldata;
for i=1:respno,
```

```
   alldata(:,i)=temp2(:,respno-i+1);
 end
 %
 % High Pass Filter
 %
 tend=(samples-1)/fs;
 t=0:(1/fs):tend;
 repeats=0;
 no_of_tests = size(alldata,2)-repeats;
 m0 = [0.001 0.001 0.001 1. 1. 1. 1. 1. 1.];
 fHz0 = [0 50 90 240 500 800 1000 1500 fs/2];
 %plot(fHz0,m0);
 f0=fHz0/(fs/2);
 [bIIR,aIIR] = yulewalk(48,f0,m0);
 fHz1 = linspace(0, fs/2, 50);
 om1 = 2*pi*fHz1;
 z = exp(sqrt(-1)*om1/fs);
 mIIR = abs(polyval(bIIR,z)./polyval(aIIR,z));
 %plot(fHz0, m0, fHz1, mIIR);
 %
 % Low Pass Filter
 %
 m02 = [1. 1. 1. 1. .001 .001 .001 .001];
 fHz02 = [0 100 500 1000 1100 1500 2000 fs/2];
 %plot(fHz0,m0);
 f02=fHz02/(fs/2);
 [bIIR2,aIIR2] = yulewalk(48,f02,m02);
 fHz12 = linspace(0, fs/2, 50);
 om12 = 2*pi*fHz12;
 z2 = exp(sqrt(-1)*om12/fs);
 mIIR2 = abs(polyval(bIIR2,z2)./polyval(aIIR2,z2));
 %plot(fHz02, m02, fHz12, mIIR2);


%%%%%%%%%%%%%%%%%%%%%%%%%%%%%%%%%%%%%%%%%%%%%%%%%%%%%%%%
%
%       FILTER experimental data
%
%%%%%%%%%%%%%%%%%%%%%%%%%%%%%%%%%%%%%%%%%%%%%%%%%%%%%%%%

if (filterno==2),
   for i=1:no_of_tests,
      filtered_data(:, i) = filter(bIIR2,aIIR2,filter(bIIR,aIIR,alldata(:, i)));
   end
   for i=1:noiseno,
      filtered_noise(:, i) = filter(bIIR2,aIIR2,filter(bIIR,aIIR,noisedata(:, i)));
   end
else
   for i=1:no_of_tests,
      filtered_data(:, i) = filter(bIIR,aIIR,alldata(:, i));
   end
   for i=1:noiseno,
```

```
      filtered_noise(:, i) = filter(bIIR,aIIR,noisedata(:, i));
    end
end


%%%%%%%%%%%%%%%%%%%%%%%%%%%%%%%%%%%%%%%%%%%%%%%%%%%%%%%%%%%%%%%%%%%%%%%%%%%%
%
%       CALCULATE Type 1 Damage Indices using all data samples
%
%%%%%%%%%%%%%%%%%%%%%%%%%%%%%%%%%%%%%%%%%%%%%%%%%%%%%%%%%%%%%%%%%%%%%%%%%%%%

temp5=filtered_data;
filtered_data(:,secure)=flipud(rot90(mean(flipud(rot90([filtered_data(:,respno-2)  filtered_data(:,respno-1)
filtered_data(:,respno)])))));
maxnoise=max(max(abs(filtered_noise)));
cutofflevel=colfactor*maxnoise;
halfcyclesamples=0.5*(fs/excfr);
for i=1:no_of_tests+1,
   i
   dsum1(i)=0;
   dsum2(i)=0;
   dsum3(i)=0;
   dsum4(i)=0;
   cutoffcount(i)=0;
   for j=endsample_of_excn:samples,
      if (abs(filtered_data(j,i))<cutofflevel),
         cutoffcount(i)=cutoffcount(i)+1;
      else
         cutoffcount(i)=0;
      end
   end
   if (cutoffcount(i)>halfcyclesamples),
      cutoff(i)=samples-cutoffcount(i);
   else
      cutoff(i)=samples;
   end
   for j=firstsample:cutoff(i),
      damage2(j,i)=sqrt((filtered_data(j,i)-filtered_data(j,secure))^2);
      damage3(j,i)=sqrt((abs(filtered_data(j,i))-abs(filtered_data(j,secure)))^2);
      damage4(j,i)=(filtered_data(j,secure)-filtered_data(j,i))^2;
      dsum1(i)=dsum1(i)+abs(filtered_data(j,i));
      dsum2(i)=dsum2(i)+damage2(j,i);
      dsum3(i)=dsum3(i)+damage3(j,i);
      dsum4(i)=dsum4(i)+damage4(j,i);
      if (j==endsample_of_excn),
         dsum1e(i)=dsum1(i);
         dsum2e(i)=dsum2(i);
         dsum3e(i)=dsum3(i);
         dsum4e(i)=dsum4(i);
      end
   end
   noused(i)=cutoff(i)-1;
```

```
    dindex2(i)=dsum2(i)/noused(i);
    dindex3(i)=dsum3(i)/noused(i);
    safetyindex(i)=sqrt(dsum4(i))/noused(i);
    dindex2e(i)=dsum2e(i)/endsample_of_excn;
    dindex3e(i)=dsum3e(i)/endsample_of_excn;
    safetyindexe(i)=sqrt(dsum4e(i))/endsample_of_excn;
    dindex2f(i)=(dsum2(i)-dsum2e(i))/(noused(i)-endsample_of_excn);
    dindex3f(i)=(dsum3(i)-dsum3e(i))/(noused(i)-endsample_of_excn);
    safetyindexf(i)=sqrt(dsum4(i)-dsum4e(i))/(noused(i)-endsample_of_excn);
end
for i=1:no_of_tests+1,
    dindex1(i)=(dsum1(secure)-dsum1(i))/noused(secure);
    dindex1e(i)=(dsum1e(secure)-dsum1e(i))/endsample_of_excn;
    dindex1f(i)=((dsum1(secure)-dsum1e(secure))-(dsum1(i)-dsum1e(i)))/(noused(secure)-endsample_of_excn);
end


%%%%%%%%%%%%%%%%%%%%%%%%%%%%%%%%%%%%%%%%%%%%%%%%%%%%%%%%%%%%%%%%%%%%
%
%       PLOT Bar Graphs for Type 1 Indices
%
%%%%%%%%%%%%%%%%%%%%%%%%%%%%%%%%%%%%%%%%%%%%%%%%%%%%%%%%%%%%%%%%%%%%

figure;
subplot(2,2,1)
bar(dindex1,'w')
title('Damage Index 1 [data=all; T.W.=1]')
ylabel('Damage Index 1 (V)');
xlabel('Clamping Force Index');
subplot(2,2,2)
bar(dindex2,'w')
title('Damage Index 2 [data=all; T.W.=1]')
ylabel('Damage Index 2 (V)');
xlabel('Clamping Force Index');
subplot(2,2,3)
bar(dindex3,'w')
title('Damage Index 3 [data=all; T.W.=1]')
ylabel('Damage Index 3 (V)');
xlabel('Clamping Force Index');
subplot(2,2,4)
bar(safetyindex,'w')
title('Damage Index 4 [data=all; T.W.=1]')
ylabel('Damage Index 4 (V)');
xlabel('Clamping Force Index');
%
figure;
subplot(2,2,1)
bar(dindex1e,'w')
title('Damage Index 1 [data=all; T.W.=2]')
ylabel('Damage Index 1 (V)');
xlabel('Clamping Force Index');
subplot(2,2,2)
```

```
bar(dindex2e,'w')
title('Damage Index 2 [data=all; T.W.=2]')
ylabel('Damage Index 2 (V)');
xlabel('Clamping Force Index');
subplot(2,2,3)
bar(dindex3e,'w')
title('Damage Index 3 [data=all; T.W.=2]')
ylabel('Damage Index 3 (V)');
xlabel('Clamping Force Index');
subplot(2,2,4)
bar(safetyindexe,'w')
title('Damage Index 4 [data=all; T.W.=2]')
ylabel('Damage Index 4 (V)');
xlabel('Clamping Force Index');
%
figure;
subplot(2,2,1)
bar(dindex1f,'w')
title('Damage Index 1 [data=all; T.W.=3]')
ylabel('Damage Index 1 (V)');
xlabel('Clamping Force Index');
subplot(2,2,2)
bar(dindex2f,'w')
title('Damage Index 2 [data=all; T.W.=3]')
ylabel('Damage Index 2 (V)');
xlabel('Clamping Force Index');
subplot(2,2,3)
bar(dindex3f,'w')
title('Damage Index 3 [data=all; T.W.=3]')
ylabel('Damage Index 3 (V)');
xlabel('Clamping Force Index');
subplot(2,2,4)
bar(safetyindexf,'w')
title('Damage Index 4 [data=all; T.W.=3]')
ylabel('Damage Index 4 (V)');
xlabel('Clamping Force Index');
%
% Titles for each experiment test case i and trial (a, b or c)
%
titles(1,:)=['Disconnected i=1 Trial A'];
titles(2,:)=['Disconnected i=1 Trial B'];
titles(3,:)=['Disconnected i=1 Trial C'];
titles(4,:)=[' Damaged i=2 Trial A  '];
titles(5,:)=[' Damaged i=2 Trial B  '];
titles(6,:)=[' Damaged i=2 Trial C  '];
titles(7,:)=[' Damaged i=3 Trial A  '];
titles(8,:)=[' Damaged i=3 Trial B  '];
titles(9,:)=[' Damaged i=3 Trial C  '];
titles(10,:)=[' Damaged i=4 Trial A  '];
titles(11,:)=[' Damaged i=4 Trial B  '];
titles(12,:)=[' Damaged i=4 Trial C  '];
titles(13,:)=[' Damaged i=5 Trial A  '];
```

```
titles(14,:)=[' Damaged i=5 Trial B  '];
titles(15,:)=[' Damaged i=5 Trial C  '];
titles(16,:)=[' Damaged i=6 Trial A  '];
titles(17,:)=[' Damaged i=6 Trial B  '];
titles(18,:)=[' Damaged i=6 Trial C  '];
titles(19,:)=['  Secure i=7 Trial A  '];
titles(20,:)=['  Secure i=7 Trial B  '];
titles(21,:)=['  Secure i=7 Trial C  '];
titles(22,:)=['    Secure i=7 avg    '];

aa=rot90([excycles/excfr excycles/excfr]);


%%%%%%%%%%%%%%%%%%%%%%%%%%%%%%%%%%%%%%%%%%%%%%%%%%%%%%%%%%%%%%%%
%
%       PLOT unfiltered responses using all data samples
%
%%%%%%%%%%%%%%%%%%%%%%%%%%%%%%%%%%%%%%%%%%%%%%%%%%%%%%%%%%%%%%%%

if (noisyflag=='y'),

grows=3;
gcols=3;
xlo=0;
xhi=1.0;
ylo=-1;
yhi=1;
bb4=rot90([ylo yhi]);
i=1;
while (i<=no_of_tests),
  figure;
  j=0;
  if ((no_of_tests-i)<grows*gcols),
    stop=no_of_tests-i+1;
  else
    stop=grows*gcols;
  end
  for k=1:stop,
    subplot(grows,gcols,k)
    plot(t,alldata(:,i),aa,bb4,'--')
    axis([xlo xhi ylo yhi]);
    set(gca,'xtick',[0. .25 .5 .75 1.]);
    j=j+1;
    if (j==1)
      ylabel('Volts');
    end
    if (j==gcols)
      j=0;
    end
    if (k>gcols*(grows-1))
      xlabel('Time (s)');
    end
```

```
      title(titles(i,:))
      i=i+1;
    end
  end

end


%%%%%%%%%%%%%%%%%%%%%%%%%%%%%%%%%%%%%%%%%%%%%%%%%%%%%%%%%%%%%%%%
%
%       DETERMINE max/min values for each cycle of each filtered response
%
%%%%%%%%%%%%%%%%%%%%%%%%%%%%%%%%%%%%%%%%%%%%%%%%%%%%%%%%%%%%%%%%

for i=1:no_of_tests+1,
  minno(i)=0;
  maxno(i)=0;
  j=1;
  prevmin=0;
  prevmax=0;
  clear jjmin;
  clear jjmax;
  while (filtered_data(j,i)==filtered_data(j+1,i)),
    j=j+1;
  end
  if (filtered_data(j,i)>filtered_data(j+1,i)),
    flag='max'
  else
    flag='min'
  end
  while (j<(samples-1)),
    while (((filtered_data(j,i)>=filtered_data(j+1,i))&(flag=='max'))|((filtered_data(j,i)<=filtered_data(j+1,i))&
              (flag=='min'))&(j<(samples-1))),
      j=j+1;
    end
    if (((filtered_data(j,i)<filtered_data(j+1,i))&(flag=='max'))&(j<(samples-1))),
      if (filtered_data(j,i)<=0),
        minno(i)=minno(i)+1;
        jjmin(minno(i))=j;
        prevmin=filtered_data(j,i);
        flag='min';
      else
        localmin=filtered_data(j,i);
        while(((filtered_data(j,i)<=prevmax)&(filtered_data(j,i)>=localmin))&(j<(samples-1))),
          j=j+1;
        end
        if (filtered_data(j,i)>prevmax)
          maxno(i)=maxno(i)-1;
          flag='min';
        end
      end
    end
```

```
        if (((filtered_data(j,i)>filtered_data(j+1,i))&(flag=='min'))&(j<(samples-1))),
          if (filtered_data(j,i)>=0),
            maxno(i)=maxno(i)+1;
            jjmax(maxno(i))=j;
            prevmax=filtered_data(j,i);
            flag='max';
          else
            localmax=filtered_data(j,i);
            while (((filtered_data(j,i)>=prevmin)&(filtered_data(j,i)<=localmax))&(j<(samples-1))),
              j=j+1;
            end
            if (filtered_data(j,i)<prevmin)
              minno(i)=minno(i)-1;
              flag='max';
            end
          end
        end
      end
      i
      for k=1:minno(i),
        minindex(k,i)=jjmin(k);
        minmat(k,i) = filtered_data(minindex(k,i),i);
      end
      for k=1:maxno(i),
        maxindex(k,i)=jjmax(k);
        maxmat(k,i) = filtered_data(maxindex(k,i),i);
      end
    end


%%%%%%%%%%%%%%%%%%%%%%%%%%%%%%%%%%%%%%%%%%%%%%%%%%%%%%%%
%
%       PLOT filtered responses using cycle maxima/minima only
%
%%%%%%%%%%%%%%%%%%%%%%%%%%%%%%%%%%%%%%%%%%%%%%%%%%%%%%%%

grows=3;
gcols=3;
xlo=0;
xhi=1.0;
ylo=-1*(max(max(filtered_data)))*1.1;
yhi=max(max(filtered_data))*1.1;
ymax=0.;
while(yhi>ymax),
  if(yhi>ymax),
    ymax=ymax+.2;
  end
end
yhi=ymax;
ylo=-ymax;
bb3=rot90([ylo yhi]);
i=1;
```

```
while (i<=no_of_tests+1),
  figure;
  j=0;
  if ((no_of_tests-i+1)<(grows*gcols)),
    stop=no_of_tests-i+2;
  else
    stop=grows*gcols;
  end
  for k=1:stop,
    subplot(grows,gcols,k)
    plot(maxindex(1:maxno(i),i)/fs,filtered_data(maxindex(1:maxno(i),i),i),minindex(1:minno(i),i)/fs,
            filtered_data(minindex(1:minno(i),i),i),aa,bb3,'--')
    axis([xlo xhi ylo yhi]);
    set(gca,'xtick',[0. .25 .5 .75 1.]);
    set(gca,'ytick',[ylo ylo/2 0. yhi/2 yhi]);
    j=j+1;
    if (j==1)
      ylabel('Volts');
    end
    if (j==gcols)
      j=0;
    end
    if (k>gcols*(grows-1))
      xlabel('Time (s)');
    end
    title(titles(i,:))
    i=i+1;
  end
end


%%%%%%%%%%%%%%%%%%%%%%%%%%%%%%%%%%%%%%%%%%%%%%%%%%%%%%%%%%%%%%%%%%%%%%%%%%%%%%
%
%       CALCULATE Type 1 damage indices (based on cycle max/min values only)
%
%%%%%%%%%%%%%%%%%%%%%%%%%%%%%%%%%%%%%%%%%%%%%%%%%%%%%%%%%%%%%%%%%%%%%%%%%%%%%%

for i=1:no_of_tests+1,
  dsum1m(i)=0;
  dsum2m(i)=0;
  dsum3m(i)=0;
  dsum4m(i)=0;
  i
  k=1;
  cutoffcountm(i)=0;
  for k=excycles:min([maxno minno]),
    if ((abs(filtered_data(maxindex(k,i),i))<cutofflevel)&(abs(filtered_data(minindex(k,i),i))<cutofflevel)),
      cutoffcountm(i)=cutoffcountm(i)+1;
    else
      cutoffcountm(i)=0;
    end
  end
```

```
cutoffm(i)=min([maxno(i) minno(i)])-cutoffcountm(i);
for k=firstmaxmin:cutoffm(i),
  damage2max(k,i)=sqrt((filtered_data(maxindex(k,i),i)-filtered_data(maxindex(k,secure),secure))^2);
  damage3max(k,i)=sqrt((abs(filtered_data(maxindex(k,i),i))-abs(filtered_data(maxindex(k,secure),secure)))^2);
  damage4max(k,i)=(filtered_data(maxindex(k,secure),secure)-filtered_data(maxindex(k,i),i))^2;
  damage2min(k,i)=sqrt((filtered_data(minindex(k,i),i)-filtered_data(minindex(k,secure),secure))^2);
  damage3min(k,i)=sqrt((abs(filtered_data(minindex(k,i),i))-abs(filtered_data(minindex(k,secure),secure)))^2);
  damage4min(k,i)=(filtered_data(minindex(k,secure),secure)-filtered_data(minindex(k,i),i))^2;
  dsum1m(i)=dsum1m(i)+abs(filtered_data(maxindex(k,i),i))+abs(filtered_data(minindex(k,i),i));
  dsum2m(i)=dsum2m(i)+damage2max(k,i)+damage2min(k,i);
  dsum3m(i)=dsum3m(i)+damage3max(k,i)+damage3min(k,i);
  dsum4m(i)=dsum4m(i)+damage4max(k,i)+damage4min(k,i);
  if (k==endcycle_of_excn),
    dsum1me(i)=dsum1m(i);
    dsum2me(i)=dsum2m(i);
    dsum3me(i)=dsum3m(i);
    dsum4me(i)=dsum4m(i);
  end
end
nomaxmin(i)=2*cutoffm(i);
dindex2m(i)=dsum2m(i)/nomaxmin(i);
dindex3m(i)=dsum3m(i)/nomaxmin(i);
safetyindexm(i)=sqrt(dsum4m(i))/nomaxmin(i);
dindex2me(i)=dsum2me(i)/endcycle_of_excn;
dindex3me(i)=dsum3me(i)/endcycle_of_excn;
safetyindexme(i)=sqrt(dsum4me(i))/endcycle_of_excn;
dindex2mf(i)=(dsum2m(i)-dsum2me(i))/(nomaxmin(i)-endcycle_of_excn);
dindex3mf(i)=(dsum3m(i)-dsum3me(i))/(nomaxmin(i)-endcycle_of_excn);
safetyindexmf(i)=sqrt(dsum4m(i)-dsum4me(i))/(nomaxmin(i)-endcycle_of_excn);
end
for i=1:no_of_tests+1,
  dindex1m(i)=(dsum1m(secure)-dsum1m(i))/nomaxmin(secure);
  dindex1me(i)=(dsum1me(secure)-dsum1me(i))/endcycle_of_excn;
  dindex1mf(i)=((dsum1m(secure)-dsum1me(secure))-(dsum1m(i)-dsum1me(i)))/(nomaxmin(secure)
            -endcycle_of_excn);
end

%%%%%%%%%%%%%%%%%%%%%%%%%%%%%%%%%%%%%%%%%%%%%%%%%%%%%%%%%%%%%%%%%%%%%%%%%%%%%%%%%%%%%%%%%%%%%%%%%%
%
%     PLOT Bar Graphs for Type 1 Damage Indices (based on cycle max/min only)
%
%%%%%%%%%%%%%%%%%%%%%%%%%%%%%%%%%%%%%%%%%%%%%%%%%%%%%%%%%%%%%%%%%%%%%%%%%%%%%%%%%%%%%%%%%%%%%%%%%%

figure;
subplot(2,2,1)
bar(dindex1m,'w')
title('Damage Index 1 [data=max/min; T.W.=1]')
ylabel('Damage Index 1 (V)');
xlabel('Clamping Force Index');
subplot(2,2,2)
bar(dindex2m,'w')
title('Damage Index 2 [data=max/min; T.W.=1]')
```

```
ylabel('Damage Index 2 (V)');
xlabel('Clamping Force Index');
subplot(2,2,3)
bar(dindex3m,'w')
title('Damage Index 3 [data=max/min; T.W.=1]')
ylabel('Damage Index 3 (V)');
xlabel('Clamping Force Index');
subplot(2,2,4)
bar(safetyindexm,'w')
title('Damage Index 4 [data=max/min; T.W.=1]')
ylabel('Damage Index 4 (V)');
xlabel('Clamping Force Index');
%
figure;
subplot(2,2,1)
bar(dindex1me,'w')
title('Damage Index 1 [data=max/min; T.W.=2]')
ylabel('Damage Index 1 (V)');
xlabel('Clamping Force Index');
subplot(2,2,2)
bar(dindex2me,'w')
title('Damage Index 2 [data=max/min; T.W.=2]')
ylabel('Damage Index 2 (V)');
xlabel('Clamping Force Index');
subplot(2,2,3)
bar(dindex3me,'w')
title('Damage Index 3 [data=max/min; T.W.=2]')
ylabel('Damage Index 3 (V)');
xlabel('Clamping Force Index');
subplot(2,2,4)
bar(safetyindexme,'w')
title('Damage Index 4 [data=max/min; T.W.=2]')
ylabel('Damage Index 4 (V)');
xlabel('Clamping Force Index');
%
figure;
subplot(2,2,1)
bar(dindex1mf,'w')
title('Damage Index 1 [data=max/min; T.W.=3]')
ylabel('Damage Index 1 (V)');
xlabel('Clamping Force Index');
subplot(2,2,2)
bar(dindex2mf,'w')
title('Damage Index 2 [data=max/min; T.W.=3]')
ylabel('Damage Index 2 (V)');
xlabel('Clamping Force Index');
subplot(2,2,3)
bar(dindex3mf,'w')
title('Damage Index 3 [data=max/min; T.W.=3]')
ylabel('Damage Index 3 (V)');
xlabel('Clamping Force Index');
subplot(2,2,4)
```

```
bar(safetyindexmf,'w')
title('Damage Index 4 [data=max/min; T.W.=3]')
ylabel('Damage Index 4 (V)');
xlabel('Clamping Force Index');


%%%%%%%%%%%%%%%%%%%%%%%%%%%%%%%%%%%%%%%%%%%%%%%%%%%%%%%%%%%%%%%%%%%%%
%
%        PLOT Bar Graphs for Type 2 and 3 Damage Indices
%
%%%%%%%%%%%%%%%%%%%%%%%%%%%%%%%%%%%%%%%%%%%%%%%%%%%%%%%%%%%%%%%%%%%%%

figure;
subplot(2,2,1)
bar(noused,'w')
title('Decay Duration to Cutoff Level')
ylabel('Decay Duration (samples)');
xlabel('Clamping Force Index');
subplot(2,2,2)
bar(max(filtered_data),'w')
title('Maximum Response Amplitude')
ylabel('Maximum Value (V)');
xlabel('Clamping Force Index');


%%%%%%%%%%%%%%%%%%%%%%%%%%%%%%%%%%%%%%%%%%%%%%%%%%%%%%%%%%%%%%%%%%%%%
%
%        WRITE data to '.out' files
%
%%%%%%%%%%%%%%%%%%%%%%%%%%%%%%%%%%%%%%%%%%%%%%%%%%%%%%%%%%%%%%%%%%%%%

if (outputflag=='y'),

dindexdata(1:8,:)=[dindex1
dindex2
dindex3
safetyindex
dindex1m
dindex2m
dindex3m
safetyindexm];
dindexdata(9:16,:)=[dindex1e
dindex2e
dindex3e
safetyindexe
dindex1me
dindex2me
dindex3me
safetyindexme];
dindexdata(17:24,:)=[dindex1f
dindex2f
```

```
dindex3f
safetyindexf
dindex1mf
dindex2mf
dindex3mf
safetyindexmf];
dindexdata(25:26,:)=[max(filtered_data)
noused];
%
z='%15.12f ';
d1='c:\arob\finalp~1\output\';
z7=[z z z z z z z];
n1='\n';
frmt2=[z z z z z z z7 z7 z7 n1];
frmt=[z7 z7 z7 n1];
fileadd=fname(5:6);
%
fid=fopen([d1 'alldat' fileadd '.out'],'w');
count=fprintf(fid,[z frmt],flipud(rot90(filtered_data)))
fclose(fid)
fid=fopen([d1 'aldatn' fileadd '.out'],'w');
count=fprintf(fid,frmt,flipud(rot90(alldata)))
fclose(fid)
fid=fopen([d1 'max' fileadd '.out'],'w');
count=fprintf(fid,[z frmt],flipud(rot90(maxmat)))
fclose(fid)
fid=fopen([d1 'min' fileadd '.out'],'w');
count=fprintf(fid,[z frmt],flipud(rot90(minmat)))
fclose(fid)
fid=fopen([d1 'damind' fileadd '.out'],'w');
count=fprintf(fid,frmt2,dindexdata)
fclose(fid)

end
```

Appendix D

C - Program

```
/*****************************************************************************/
/*                                                                           */
/*  C-Program for exciting beam and measuring its response in terms of sensor voltage  */
/*  Excitation: sinusoidal waveform; frequency = 361 Hz; number of cycles = 50; amplitude = 10V  */
/*  Sampling freq. = 5776 Hz                                                 */
/*                                                                           */
 /*****************************************************************************/

/*******************************************/
/*        Declare input / output functions          */
/*******************************************/

float ds2002(long base, long channel);
void  ds2101(long base,long channel,float value);
#include <c:\c30tools\math.h>
#include <c:\c30tools\stdio.h>

/*********************************/
/*        Declare  variables          */
/*********************************/

const float f = 361.;    /* Frequency of excitation  */
const int cycles = 50;  /* Number of excitation cycles  */
const float mag10 = 1.;  /* Magnitude of excitation divided by 10 */
float ht;            /* Sampling time */
long int j=0;
long int i=0;
long int k=0;
float excite;         /* Excitation function */
float gain1;          /* Gain adjustment */
```

```
float tdelay;
int samples_per_cycle;
int half_cycle;
float mes_sgn_f=0.; /* Initialize */

/*********************************/
/*        Interrupt loop         */
/*********************************/

c_int10()
{
  ht=1./(5776.);
  tdelay=10.*(1/ht);
  samples_per_cycle=1/(ht*f);
  half_cycle=samples_per_cycle/2;
  if (j>tdelay)                    /* after 10 second delay */
  {
    asm("      trapu   27");  /* call TRACE30 */

/*****************************************************/
/*        Send signal to Actuator                    */
/*****************************************************/

     excite=mag10*sin(2*3.1416*f*ht*i);
     if(j>(tdelay+cycles*samples_per_cycle)) excite=0.;
     ds2101(0x00000090,0x00000004,excite);
     i=i+1;

/*****************************************/
/*      Read signal from sensor (TRACE30)  */
/*****************************************/

     gain1=27.1;    /* gain adjustment so TRACE30 beam response agrees with oscilloscope beam response  */
     mes_sgn_nf = gain1*ds2002(0x00000020, 0x0000000b);
  }
  j=j+1;
}

/*******************************************/
/*        Main program (loop)              */
/*******************************************/

void init();
void timer1(float time);
main()
{
  init();
  timer1(1./5776.));
  for (;;)
  ;
}
```